A COMPREHENSIVE MODEL OF ELECTRIC-FIELD-ENHANCED JUMPING-DROPLET CONDENSATION ON SUPERHYDROPHOBIC SURFACES

BY

PATRICK BIRBARAH

THESIS

Submitted in partial fulfillment of the requirements
for the degree of Master of Science in Mechanical Engineering
in the Graduate College of the
University of Illinois at Urbana-Champaign, 2016

Urbana, Illinois

Advisor:

Assistant Professor Nenad Miljkovic

ABSTRACT

Superhydrophobic micro/nanostructured surfaces for dropwise condensation have recently received significant attention due to their potential to enhance heat transfer performance by shedding positively charged water droplets *via* coalescence-induced droplet jumping at length scales below the capillary length, and allowing the use of external electric fields to enhance droplet removal and heat transfer, in what has been termed electric-field-enhanced (EFE) jumping-droplet condensation. However, achieving optimal EFE conditions for enhanced heat transfer requires capturing the details of transport processes that is currently lacking. While a comprehensive model has been developed for condensation on micro/nanostructured surfaces, it cannot be applied for EFE condensation due to the dynamic droplet-vapor-electric field interactions. In this work, I developed a comprehensive physical model for EFE condensation on superhydrophobic surfaces by incorporating individual droplet motion, electrode geometry, jumping frequency, field strength, and condensate vapor-flow dynamics. As a first step towards my model, I simulated jumping droplet motion with no external electric field, and validated my theoretical droplet trajectories to experimentally obtained trajectories, showing excellent temporal and spatial agreement. I then incorporated the external electric field into my model and considered the effects of jumping droplet size, electrode size and geometry, condensation heat flux, and droplet jumping direction. My model suggests that smaller jumping droplet sizes and condensation heat fluxes require less work input to be removed by the external fields. Furthermore, the results suggest that EFE electrodes can be optimized such that the work input is minimized depending on the condensation heat flux. To analyze overall efficiency, I defined an incremental coefficient-of-performance and showed that it is very high (~10^6) for EFE

condensation. I finally proposed mechanisms for condensate collection which would ensure continuous operation of the EFE system, and which can scalably be applied to industrial condensers. This work provides a comprehensive physical model of the EFE condensation process, and offers guidelines for the design of EFE systems to maximize heat transfer.

ACKNOWLEDGMENTS

I would like to acknowledge my academic advisor Professor Nenad Miljkovic for his continuous support which was essential for the completion of this work. I gratefully acknowledge Professor Evelyn N. Wang of MIT for providing me with the experimental video for my droplet trajectory model validations. I also gratefully acknowledge funding support from the Air Conditioning and Refrigeration Center (ACRC), an NSF-founded I/UCRC at UIUC. Finally I would like to thank my family in Lebanon for the support they provide me continuously in my professional career.

TABLE OF CONTENTS

LIST OF SYMBOLS

COP_{inc}	Incremental coefficient of performance
COP	Coefficient of performance
μ_{v}	Dynamic viscosity of water vapor
μ_{w}	Dynamic viscosity of liquid water
u_{v}	Vapor velocity
$u_{\text{d,x}}$	Droplet velocity in x-direction
$u_{\text{d,y}}$	Droplet velocity in y-direction
$a_{\text{d,x}}$	Droplet acceleration in x-direction
$a_{\text{d,y}}$	Droplet acceleration in y-direction
R_{d}	Droplet radius
ρ_{w}	Water density
ρ_{v}	Water vapor density
g	Gravitational constant
Re	Reynolds Number
Bo	Bond number
Oh	Ohnesorge number

We	Weber number
Ca	Capillary number
$\dot{m}_c''$	Mass flux of condensate
$\dot{m}_v''$	Mass flux of vapor
q''	Heat flux
q''_{crit}	Critical heat flux
q''_E	Heat flux with application of electric field
q''_0	Heat flux without application of electric field
h_{fg}	Latent heat of vaporization of water
m	Mass of droplet
C_D	Drag Coefficient
γ	Surface tension of water
E_x	Electric Field in x-direction
E_y	Electric Field in y-direction
q_d	Droplet charge
V	Voltage
V_{crit}	Critical voltage for droplet arrival to electrode

I''	Current density (per unit area)
s	Spacing of parallel electrodes
r	Radial position
R_1	Radius of inner electrode
R_2	Radius of outer electrode
A_{eff}	Effective surface area of electrode
n	Number of droplets per m^2
$\dot{N}''_{\text{jump}}$	Number of droplets jumping per unit area
τ	Time between successive jumps
F_G	Gravitational force
F_D	Drag force
F_E	Electrostatic force
$LMTD$	Log mean temperature difference
dq	Incremental heat flux
dw	Incremental work

CHAPTER 1: INTRODUCTION

1.1. Jumping Droplet Condensation and External Electric Fields

Condensation of water vapor is a ubiquitous process utilized in nature and industry. Dropwise condensation on non-wetting surfaces has received much attention over the past century due to its potential to enhance heat transfer by 500-1000% compared to filmwise condensation.[1-10] More recently, researchers have discovered that when small microdroplets (~10-100 μm) condense and coalesce on a suitably designed superhydrophobic surface, the merged droplet can jump away from the surface irrespective of gravity due to surface-to-kinetic energy transfer.[11-16] This phenomenon has been termed jumping-droplet condensation and has been shown to further enhance heat transfer by up to 30% when compared to classical dropwise condensation due to a larger population of microdroplets which more efficiently transfer heat to the surface.[17] A number of works have since fabricated superhydrophobic nanostructured surfaces to achieve spontaneous droplet removal[18-28] for a variety of applications including self-cleaning,[29-31] thermal diodes,[30, 32] anti-icing,[33-36] vapor chambers,[37] electrostatic energy harvesting,[38-40] and condensation heat transfer enhancement.[41-52]

However, heat transfer enhancement can be limited by droplet return to the surface due to (1) gravitational force (*i.e.*, horizontally aligned condensing surface with jumping occurring on top) (2) entrainment in a bulk convective vapor flow occurring adjacent to the condensing surface (*i.e.*, due to buoyancy effects on vapor near the surface), and (3) entrainment in the local condensing vapor flow toward the surface (*i.e.*, the flow required for mass conservation of the condensing vapor).[17, 37] The first two return mechanisms (gravity and bulk vapor flow) can be mitigated with suitable geometric design of the macroscale condensing surface and

vapor supply. However, the third return mechanism (local vapor flow) is more difficult to eliminate due to the need to conserve mass of the condensing vapor flowing towards the surface. Although previous studies have experimentally characterized the effects of gravitational return,[53-54] further study of local vapor flow entrainment on droplet return and its effect on heat transfer is needed. An improved physical understanding will not only enhance heat transfer but prevent progressive surface flooding and extend high performance condensation operational time due to the reduction in large pinned droplets on the condensing surface.

Meanwhile, researchers have recently discovered and exploited the fact that jumping droplets attain a positive charge (~ +10 fC) after departing the superhydrophobic surface due to electric-double-layer charge separation at the coating-droplet interface.[40] This discovery has allowed for the development of electric-field-enhanced (EFE) condensation, whereby an external electric field was used to enhance the removal of jumping droplets from a radial (tube) condensing surface by counteracting the three droplet return mechanisms described above.[55] Through the elimination of droplet return, a heat transfer enhancement of ≈100% was experimentally demonstrated, compared to state-of-the-art dropwise condensing surfaces.

Although the previous studies have been instrumental at demonstrating EFE condensation, understanding of the effects of surface/electrode geometry and field parameters on droplet removal is currently lacking. In this study, I develop a comprehensive model of EFE condensation to study the critical electric fields needed for complete removal of charged jumping droplets, considering the effect of different parameters such as the size of the

jumping droplets, the geometry and orientation of the charged electrodes/condensing surfaces, as well as the condensation heat fluxes.

1.2. Scope of Research Work

I begin by validating the jumping droplet mechanisms *via* a jumping droplet trajectory analysis (without EFE condensation). By expanding my model to include external electric fields, I subsequently show that EFE condensation can indeed be optimized *via* suitable electrode design and consideration of condensing conditions. To better understand the efficiency of EFE condensation, I use my model to show that the incremental coefficient of performance (COP_{inc}), defined as the ratio of the heat transfer enhancement due to removal of droplets to the power required to maintain the external electric field, is heat flux dependent, and ~10^6 for the condensation conditions typically seen in industry. The high COP_{inc} makes EFE condensation inherently advantageous when compared to jumping-droplet condensation without electric fields, and translates to an overall system COP enhancement, defined as the ratio of the overall condensation heat transfer to the work required to supply the cooling water and maintain a fixed electric potential, directly proportional to the EFE heat transfer enhancement (≈+50%). Lastly, I utilize my developed model to provide guidelines for designing electrodes capable of efficiently collecting the removed droplets while maintaining operational integrity. This work offers design guidelines for EFE condensation applications and insights into new avenues for performance improvement and optimization of jumping-droplet condensation.

CHAPTER 2: THEORY

2.1. Jumping Droplet Condensation Critical Heat Flux

Two fundamentally separate limitations exist for jumping droplet heat transfer. The first one, termed nucleation mediated flooding, is characterized by the saturation of the condensing surface with nucleation sites at elevated supersaturations.[56] As the nucleation density increases, droplet coalescence within unit cells of the surface structures do not allow the formation of discrete droplets which are able to coalesce and jump. Although detrimental to heat transfer, surface flooding can be avoided through the suitable design of superhydrophobic surfaces, either by the careful spatial control of nucleation sites,[57-60] or by the reduction of structure length scale.[41-42]

The second limitation, termed progressive flooding, is characterized by the entrainment of droplets in the local condensing vapor flow back toward the surface.[38, 55] Upon return, droplets can coalesce again, become larger in size, and impede heat transfer until they either jump again or finally shed due to gravity.[21-22, 53] This poses the problem of removing the droplets from the condensing surface at the microscale in order to enhance heat transfer. Naturally, jumping droplets cannot be removed if the condensing surface is oriented upwards (jumping against gravity). The droplets can be shed by gravity if the surface is oriented downwards (inclined surfaces would exhibit an intermediate behavior between these two limits). However, for downward facing surfaces, progressive flooding still exists at high heat fluxes. To obtain an estimate of the upper bound of the progressive flooding critical heat flux, I write the equation governing the motion of the droplet at the point of return (where the drag is only due to the vapor

flow). By neglecting the effect of the droplet's inertia for small increments of velocity, I can write a balance between the drag force and the gravitational force:

$$6\pi\mu_{\mathrm{v}}u_{\mathrm{v}}R_{\mathrm{d}} \approx \frac{4}{3}\pi {R_{\mathrm{d}}}^{3}\rho_{\mathrm{w}}g, \tag{1}$$

where μ_{v} = 10.3 μPa·s is the water vapor viscosity, u_{v} is the vapor velocity, R_{d} is the droplet radius, ρ_{w} = 992 kg/m^3 is the water density, and g = 9.81 m/s^2 is the gravitational constant. I note that the properties of water and vapor throughout the manuscript were taken at saturation conditions corresponding to 40°C commonly seen in industrial condenser applications. I approximated the drag on the droplet as Stokes flow[61] over a sphere since the Reynolds number was much less than 1 ($\mathrm{Re} = 2\rho_{\mathrm{v}}u_{\mathrm{v}}R_{\mathrm{d}}/\mu_{\mathrm{v}}$ ~ 0.1, where ρ_{v} = 0.05 kg/m^3 is the water vapor density).

The vapor flow velocity toward the condensing surface is the result of mass conservation at steady state: the mass flow rate of condensate per unit area $\dot{m}_{\mathrm{c}}''$ is equal to the mass flow rate per unit area of vapor near the surface $\dot{m}_{\mathrm{v}}''$. Using the latent heat of phase change per unit area, $q'' = \dot{m}_{\mathrm{c}}''h_{\mathrm{fg}}$, where h_{fg} = 2407 kJ/kg is the latent heat of phase change of water, and the water vapor mass flow rate $\dot{m}_{\mathrm{v}}'' = \rho_{\mathrm{v}}u_{\mathrm{v}}$, I obtain the vapor velocity in terms of the heat flux:

$$u_{\mathrm{v}} = \frac{q''}{\rho_{\mathrm{v}}h_{\mathrm{fg}}} \tag{2}$$

Combining Eqns. (1) and (2), I obtain the progressive flooding critical heat flux, ${q''}_{\mathrm{crit}}$:

$${q''}_{\mathrm{crit}} \approx \frac{2}{9}\frac{\rho_{\mathrm{w}}\rho_{\mathrm{v}}h_{\mathrm{fg}}{R_{\mathrm{d}}}^{2}g}{\mu_{\mathrm{v}}} \tag{3}$$

Figure 1 shows the progressive flooding heat flux as a function of jumping droplet radius. As the droplet radius increases, the critical heat flux increases due to the larger gravitational body force counteracting the vapor drag force. For droplets up to 100 μm in radius, the maximum heat flux does not exceed 10 W/cm^2, representing a limit for the desired performance if no external body forces are applied to the departing droplets. For cylindrical and spherical condensing surfaces I expect a similar order of magnitude for the critical heat flux, with larger values due to the decaying vapor flow velocity away from the surface. The calculated critical heat flux (Eq. (3)) matches with previous scaling for maximum vapor chamber performance.[37]

In order to further enhance jumping droplet condensation heat transfer beyond the limited threshold of ≈10 W/cm^2, additional body forces such as those provided with external electric fields (EFE condensation) must be utilized in order to effectively delay the onset of the critical heat flux. To better understand EFE condensation process, I developed a model for charged jumping droplet motion during condensation in electric fields.

2.2. Jumping Droplet Model

To develop a comprehensive high fidelity model for EFE condensation, I first began by modeling the trajectory of a single jumping droplet originating from a superhydrophobic flat plate facing upward and comparing my model trajectory to an experimental trajectory captured in a previous study.[12] The experimental trajectory was obtained through condensation of water vapor on a superhydrophobic copper sample coated with SPF functionalized CuO nanostructures (for CuO nanostructuring and SPF functionalization

details, please see references 17 and 55, respectively). The flat geometry of the sample allowed for simultaneous high-speed imaging of droplet jumping against gravity. To visualize the behavior, the CuO samples were tested in a controlled condensation chamber interfaced with a high-speed camera (see Supporting Information section of reference 12). Figure 2a shows the free body diagram on a droplet jumping upward. By balancing the forces acting on the droplet, I obtain the following differential equations governing the motion of the droplet in the x and y directions:

$$ma_{\mathrm{d,x}} = -\frac{1}{2}\rho_{\mathrm{v}}\pi {R_{\mathrm{d}}}^2 C_{\mathrm{D}}(u_{\mathrm{d,x}})^2 sgn(u_{\mathrm{d,x}})\,, \tag{4}$$

$$ma_{\mathrm{d,y}} = -\frac{1}{2}\rho_{\mathrm{v}}\pi {R_{\mathrm{d}}}^2 C_{\mathrm{D}}(u_{\mathrm{d,y}} + u_{\mathrm{v,y}})^2 sgn(u_{\mathrm{d,x}} + u_{\mathrm{v,x}}) - mg\,, \tag{5}$$

where $\overrightarrow{u_{\mathrm{v}}}$ is the vapor velocity (Eq. (2)), and $\overrightarrow{a_{\mathrm{d}}}$ is the droplet acceleration, m is the mass of the droplet ($m = (4/3)\pi {R_{\mathrm{d}}}^3 \rho_{\mathrm{w}}$), and C_{D} is the Reynolds number dependent drag coefficient.[62] The symbol *sgn* is used to define the sign function ($sgn(u_{\mathrm{d,x}}) = +1$ for $u_{\mathrm{d,x}} > 0$, and $sgn(u_{\mathrm{d,x}}) = -1$ for $u_{\mathrm{d,x}} < 0$). I assumed that, due to the relatively small size of departing droplets (~10-100 μm), the shape of droplets remained spherical during flight. This assumption is justified given that the Bond, Webber, and Capillary numbers are all much less than one ($\mathrm{Bo} = \rho_w g {R_{\mathrm{d}}}^2/\gamma \ll 1, \mathrm{We} = \rho_{\mathrm{v}} {U_{\mathrm{v}}}^2 R_{\mathrm{d}}/\gamma \ll 1, \mathrm{Ca} = \mu_{\mathrm{v}} U_{\mathrm{v}}/\gamma \ll 1$, where γ = 73 mN/m is the water surface tension).[63]

In order to numerically solve the two second order ordinary differential equations (Eqns. (4) and (5)), I utilized the initial position and velocity vectors obtained from the experimental droplet trajectory. The droplet radius was experimentally measured from the video to be $R_{\mathrm{d,exp}} \approx 14 \pm 4$ μm. In order to match the experimental trajectory, the

only parameter that required fitting was the condensation heat flux, which in this case was too low to experimentally measure with certainty. Figure 2b shows the simulated and experimental trajectories for a droplet of R_d = 14 μm. The obtained trajectories matched both in position and in time with the experimental trajectories, which shows that the model of the jumping droplet is indeed valid. The heat flux used to fit the trajectory was $q'' = 0.01$ W/cm^2, which is in good agreement with the small estimated heat flux used during the experiments.[12]

2.3. Electric-Field-Enhanced (EFE) Condensation Model

After validating the basic physics that govern the jumping droplet motion, I added the effects of external electric fields to my model, *i.e.* an electrostatic force term to Eqns. (4) and (5), which is used to remove the positively charged jumping droplets from the superhydrophobic surface. This electric field is established between a positively charged inner electrode (the superhydrophobic condensing surface) and a negatively charged outer electrode, forming a capacitor. The equations of motions now become:

$$ma_{d,x} = -\frac{1}{2}\rho_v \pi {R_d}^2 C_D (u_{d,x} + u_{v,x})^2 sgn(u_{d,x} + u_{v,x}) + q_d E_x \,, \quad (6)$$

$$ma_{d,y} = -\frac{1}{2}\rho_v \pi {R_d}^2 C_D (u_{d,y} + u_{v,y})^2 sgn(u_{d,y} + u_{v,y}) - mg + q_d E_y, \quad (7)$$

where q_d represents droplet electrostatic charge (q_d = 10 fC for R_d < 7 μm, and $q_d = (17x10^{-6})(4\pi {R_d}^2)$ for R_d > 7 μm (Coulombs)),[40] and $\vec{E}$ is the electric field at each position (x,y). It is important to note that the droplet electrostatic charge, q_d, is hydrophobic coating material dependent. For this model, I have chosen an SPF fluoropolymer coating as the material.[40] My model assumes that the condensing surface

is superhydrophobic and suitably designed to enable droplet jumping.[12, 46] In addition, I assume that condensing droplets being created on the superhydrophobic surface have the partially wetting morphology,[44] similar to the CuO surface previously analyzed, allowing for enhanced heat transfer to be achieved.[17]

Three different capacitor geometries were considered: cylindrical (Fig. 3a), spherical (Fig. 3a), and parallel plate (Fig. 3b). For a fixed applied voltage V, the electric field magnitude E in a parallel plate capacitor is given in terms of the electrode spacing s by $E = V/s$. For cylindrical and spherical capacitors, E is given, respectively, by the following[64]:

$$E = \frac{V}{r ln(^{R_2}/_{R_1})}, \tag{8}$$

$$E = \frac{V R_1 R_2}{r^2 (R_2 - R_1)}, \tag{9}$$

where R_1, R_2 and r are depicted in Fig. 3a.

For the cylindrical and spherical cases, the vapor flow velocity is no longer uniform since the vapor flows into smaller surface areas as r decreases from R_2 to R_1. By applying the ratio of the surface area of the inner cylinder to the surface area of a cylinder of radius r, and using Eq. (2), I obtain the vapor velocity for a cylindrical system in terms of the radial position r.

$$u_{\mathrm{v}} = \frac{q''}{\rho_{\mathrm{v}} h_{\mathrm{fg}}} \frac{R_1}{r} \tag{10}$$

Similarly, for the spherical case I obtain:

$$u_{\mathrm{v}} = \frac{q''}{\rho_{\mathrm{v}} h_{\mathrm{fg}}} \frac{{R_1}^2}{r^2} \tag{11}$$

For the three geometries considered, I studied the effect of the parameters that would affect the critical voltage, V_{crit}, between the electrodes what would enable the effective removal of droplets from the condensing surface to the outer electrode within a given unit of time. I chose to set the time reference as the time interval between two jumps for a surface of uniform droplet departing size. The number of droplets present on a 1 m^2 surface can be approximated as $n \approx [round(1/2R_{\mathrm{d}})]^2$ for an array of uniformly spaced droplets[10, 65-66] where the function $round$ rounds to the result to the nearest integer, and the number of droplets jumping unit time and per unit area, $\dot{N}''_{\mathrm{jump}}$, is given by the heat flux formula $q'' = \dot{m}''_{\mathrm{c}} h_{\mathrm{fg}}$ with $\dot{m}''_{\mathrm{c}} = \dot{N}''_{\mathrm{jump}} \rho_{\mathrm{w}} \left((4/3)\pi {R_{\mathrm{d}}}^3\right)$:

$$\dot{N}''_{\mathrm{jump}} = \frac{q''}{\rho_{\mathrm{w}} \left(\frac{4}{3}\pi {R_{\mathrm{d}}}^3\right) h_{\mathrm{fg}}} \tag{12}$$

The time between consecutive jumps is $\tau = n/\dot{N}''_{\mathrm{jump}}$, hence by substituting n and $\dot{N}''_{\mathrm{jump}}$, I obtain:

$$\tau = \frac{4\rho_{\mathrm{w}} R_{\mathrm{d}} h_{\mathrm{fg}}}{3q''} \tag{13}$$

By taking this time interval, my model ensures that the jumping droplet would reach the outer electrode by the time of the next jumping event at the same departure location. This time consideration is critical due to the fact that jumping droplets have been shown to interact mid-flight and affect each other's trajectories.[40] From an energy perspective, the critical voltage is defined as the voltage needed to remove the jumping droplet such that

it arrives at the outer electrode with zero kinetic energy. This can be considered the minimum voltage required to remove droplets.[39]

In order to obtain the droplet trajectory in the electric field, the initial condition relating the jumping velocity ($u_{\mathrm{d}}|_{t=0}$) of the droplet leaving the surface to the droplet radius (R_{d}) is needed. For water droplets of radii $R_{\mathrm{d}} > 2$ μm, coalescence is governed by an inertially limited viscous regime at low neck radii $R_{\mathrm{min}}/R_{\mathrm{d}} < \mathrm{Oh}$, where R_{min} is the radius of the neck connecting the two coalescing droplets, and Oh is the characteristic droplet Ohnesorge number defined by $\mathrm{Oh} = \mu_{\mathrm{w}}/(\rho_{\mathrm{w}}\gamma R_{\mathrm{d}})^{0.5}$ and by an inertial regime at larger neck radii ($R_{\mathrm{min}}/R_{\mathrm{d}} > \mathrm{Oh}$). Due to the relatively low Ohnesorge number, Oh ≈ 0.02 to 0.1, the majority of droplet coalescence (>90% for R_{d} = 2 μm) occurs in the inertial regime where the time scale is governed by a capillary-inertial scaling.[67] Balancing the excess surface energy and kinetic energy of the jumping droplet, I obtain the characteristic scaling for the droplet velocity[68-70]:

$$u_{\mathrm{d}}|_{t=0} = \sqrt{\frac{\gamma}{\rho_w R_d}}, \tag{14}$$

To account for the incomplete conversion of excess surface energy to kinetic energy not captured by the scaling, I introduced a proportionality constant *C*, on the right-hand side of Eq. (14). For the experiments on CuO, Eq. (14) best fits the experimental data with *C* ≈ 0.23.[12]

The effect of the applied voltage on the surface tension of water *via* electrowetting was found to be negligible for electrode spacings larger than 1 cm for voltages up to 1200 V considered here (see Appendix, Section A1).

Combining the initial condition (Eq. (14)) and the vapor flow velocity for each geometry (Eqns. (2), (10) and (11)), with the droplet equation of motion (Eqns. (4) and (5)) and using a numerical discretization with a Runge-Kutta method, I determined the droplet position in the arbitrary electric field as a function of time (t) for varying parameters (see Supplementary Information, section S.5, for the associated numerical codes).

2.4. Figures

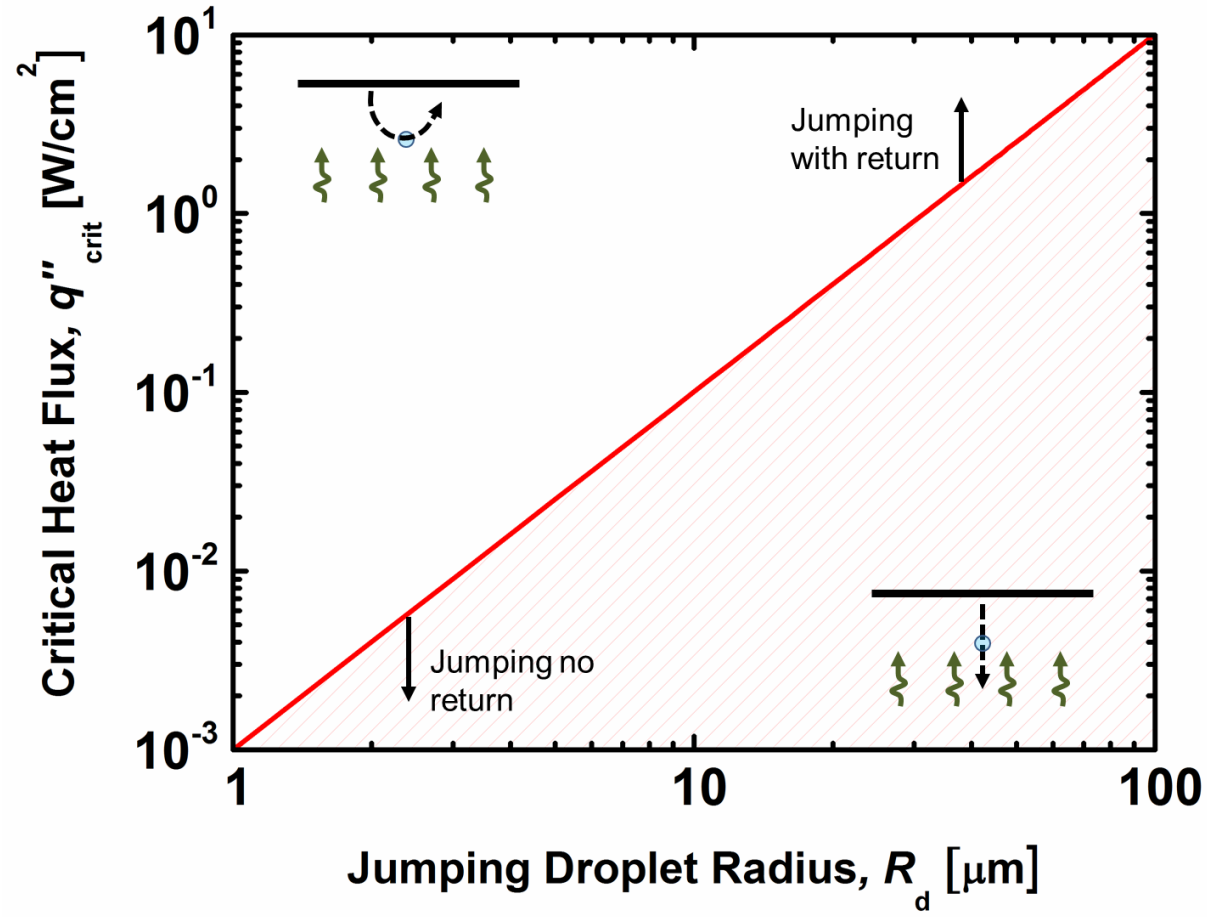

Figure 1. Theoretical maximum condensation heat flux ($q"_{crit}$) on a jumping-droplet SPF coated superhydrophobic surface as a function of jumping droplet radius R_d. The droplet is considered to be jumping downwards from a horizontal flat plate, where gravity would be most

effective in the removal of the droplet. For heat fluxes larger than $q"_{crit}$ (top left region), downward jumping droplets having radii R_d would return to the surface (inset in top left corner) due the vapor drag entrainment and result in progressive flooding of the surface with degraded heat transfer performance. For heat fluxes smaller than $q"_{crit}$ (bottom right region), downward jumping droplets having radii R_d would leave the surface (inset in bottom right corner) due gravity overcoming vapor drag entrainment.

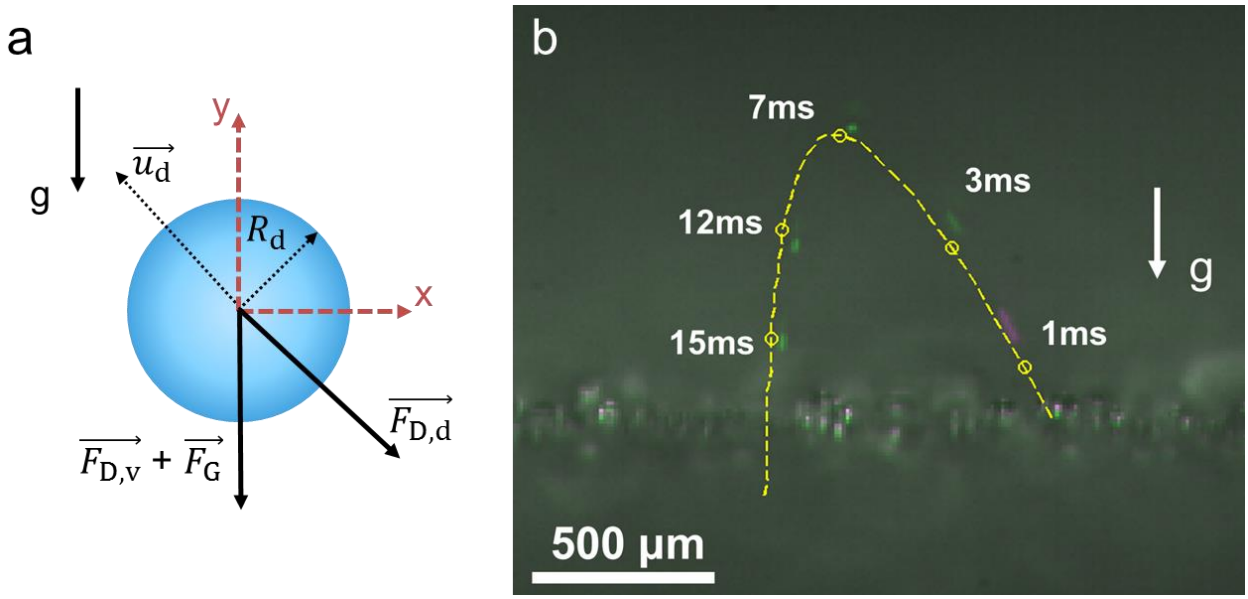

Figure 2. (a) Free body diagram on a droplet jumping upward with velocity $\overrightarrow{u_d}$ from a flat plate. $\overrightarrow{F_{D,d}}$ and $\overrightarrow{F_{D,v}}$ represent the drag force due to the droplet velocity and the drag force due to vapor flow toward the condensing surface, respectively. The gravitational force is represented by $\overrightarrow{F_G}$. (b) Theoretical (dashed yellow line) and experimental (false colored green streaks) side view trajectories of an upward jumping droplet (R_d = 14 µm) from an SPF coated superhydrophobic

copper oxide plate. The droplet jumps at an angle from the surface due to either coalescence between multiple droplets (> 2) or two droplets having disparate sizes. The actual droplet and simulated droplet are shown at different time intervals. The condensation heat flux used in the simulation was 0.01 W/cm^2. The experimental droplet locations are false colored (magenta coloring refers to the first position chosen). The simulated and experimental trajectories match in both time and position.

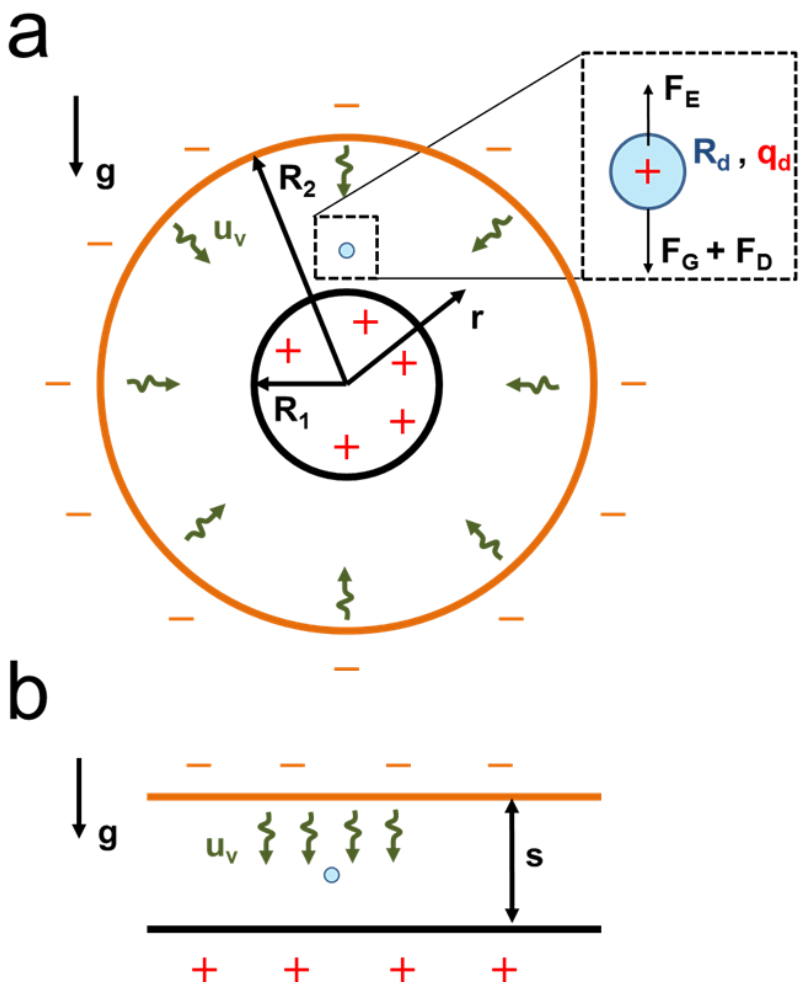

Figure 3. (a) Schematic of the electric field-enhanced (EFE) condensation on a cylindrical or spherical tube (cross section view). An electric potential is established between the outer and inner cylindrical electrodes having radii R_2 and R_1, respectively. The inner surface is a nanostructured superhydrophobic surface such as superhydrophobic copper oxide (black), while the outer electrode is a hydrophilic surface such as copper (orange). The vapor flow of velocity u_v exerts a drag on the upward jumping droplet of radius R_d and charge q_d, at a distance r from the center of the tube. The total drag force (F_D) and the gravitational force (F_G) counter the electrostatic force (F_E). (b) Parallel plate setup of the EFE condensation. The vapor flow is uniform across the spacing s of the charged electrodes.

CHAPTER 3: RESULTS AND DISCUSSION

3.1. Droplet Size

Droplet jumping on superhydrophobic surfaces has previously been shown to have a polydisperse distribution. Due to the random nature of droplet nucleation and progressive flooding effects, the droplet jumping size can range from 5 μm < R_d < 100μm. [17, 43, 53] Furthermore, the droplet electrostatic charging dynamics and jumping velocity are both droplet size dependent,[40] making a size dependent analysis critical for obtaining high fidelity results.

In order to determine a conservative value of V_{crit}, my model assumes that droplet jumping occurs in the vertical direction against gravity (for all three geometries). Figure 4a shows the critical voltage required to remove droplets as a function of jumping-droplet radius for the parallel plate case. The results show that as the droplet radius increases, a higher voltage is needed to make the droplet reach the outer electrode in order to overcome the increasing effect of gravity. For lower radii ($R_d < 20$ μm), a local maximum exists in the critical voltage centered at approximately $R_d \approx 7$ μm. In order to interpret the results, which clearly show three different regimes, I performed a scaling analysis on the forces that govern the motion of the droplet: the gravitational force F_G, the vapor drag force F_D which is given by the Stokes' drag formula ($u_d \sim 0$) at point of return of the droplet and u_v is given by Eq. (2)), and the electrostatic force F_E:

$$F_G = \frac{4}{3}\pi {R_d}^3 \rho_w g \sim \rho_w g {R_d}^3 \tag{15}$$

$$F_{\mathrm{D}} = 6\pi\mu_{\mathrm{v}}u_{\mathrm{v}}R_{\mathrm{d}} \sim \frac{u_{\mathrm{v}}q''}{\rho_{\mathrm{v}}h_{\mathrm{fg}}}R_{\mathrm{d}} \tag{16}$$

$$F_{\mathrm{E}} = q_{\mathrm{d}}\frac{V}{s} \tag{17}$$

Because the electrostatic charging of droplets is size dependent ($q_{\mathrm{d}} = 10$ fC for $R_{\mathrm{d}} < 7$ μm, and $q_{\mathrm{d}} = (17x10^{-6})(4\pi {R_{\mathrm{d}}}^2)$ for $R_{\mathrm{d}} > 7$ μm (Coulombs)),[40] two regimes exist for the electrostatic force scaling:

$$\begin{aligned} F_{\mathrm{E}} &\sim \frac{V}{s} \qquad for \;\; R_{\mathrm{d}} < 7\ \mu\mathrm{m} \\ F_{\mathrm{E}} &\sim \frac{V}{s}{R_{\mathrm{d}}}^2 \qquad for \;\; R_{\mathrm{d}} > 7\ \mu\mathrm{m} \end{aligned} \tag{18}$$

For $R_{\mathrm{d}} > 20$ μm, the electrostatic force F_{E} must balance the gravitational force F_{G} ($F_{\mathrm{E}}/F_{\mathrm{G}} \sim 1, F_{\mathrm{D}}/F_{\mathrm{G}} \sim 0$). By using Eqns. (15) and (18), I can obtain the behavior of the critical voltage in terms of R_{d}:

$$V_{crit} \sim \frac{s\rho_{\mathrm{w}}}{g}R_{\mathrm{d}} \tag{19}$$

Equation (19) explains the linear behavior observed for $R_{\mathrm{d}} > 20\ \mu$m in Fig. 4a. For the case of $R_{\mathrm{d}} < 20\ \mu$m, the vapor drag force, F_{D}, dominates the gravitational force, F_{G}, hence $F_{\mathrm{E}}/F_{\mathrm{D}} \sim 1$ and $F_{\mathrm{G}}/F_{\mathrm{D}} \sim 0$. Using Eqns. (16) and (18) I obtain the corresponding two regimes:

$$\begin{aligned} V_{\mathrm{crit}} &\sim \frac{sq''}{\rho_{\mathrm{v}}h_{\mathrm{fg}}}R_{\mathrm{d}} \qquad for \;\; R_{\mathrm{d}} < 7\ \mu\mathrm{m} \\ V_{\mathrm{crit}} &\sim \frac{su_{\mathrm{v}}q''}{\rho_{\mathrm{v}}h_{\mathrm{fg}}}\frac{1}{R_{\mathrm{d}}} \qquad for \;\; 7 < R_{\mathrm{d}} < 20\ \mu\mathrm{m} \end{aligned} \tag{20}$$

Eq. (20) describes accurately the behavior observed in the two sub-regimes shown in Fig. 4a for $R_{\mathrm{d}} < 20\ \mu$m. Note, scaling analysis to solve for V_{crit} of the cylindrical and spherical geometries is considerably more difficult to accomplish. The critical voltage behavior cannot be derived analytically since the drag and electric filed forces depend on the distance from the inner electrode, and can only be found numerically by solving the nonlinear differential equations of motion (Eqns. (6) and (7)). Figure 4b shows the results for the cylindrical and spherical geometries where the radial non linearities of the vapor flow and of the electric field lead to a slightly different behavior. Another explanation of the regimes can be done by analyzing the acceleration of the jumping droplet in terms of its radius (see Appendix, Section A2). The local maxima and minima in V_{crit} at fairly low radii indicate that an ideal droplet jumping radius can be determined from the standpoint of minimizing the power required to create the electric field. I note that for the parallel plate case, for droplets having an average radius of $R_{\mathrm{d}} = 10$ μm, I obtain a critical voltage of ≈ 200 V. This result is in good agreement with a previous experimental study that showed that voltages higher than ≈170 V for two concentric cylindrical electrodes (R_1 = 3 mm and R_2 = 2 cm) resulted in no additional enhancement in terms of heat flux.[55]

3.2. Electrode Size and Geometry

Since the electric field magnitude E depends on the spacing between the electrodes for the parallel plate case and on the inner and outer radii of the electrodes for the cylindrical and spherical cases (Eqns. (8) and (9)), I investigated the effects of varying these parameters on the critical voltage. This is deemed important due to the fact that EFE condensation has applicability ranging from the microscale (heat pipes and vapor chambers) to the macroscale (industrial condensers), making the understanding of the

effects of electrode size very important. Figure 5 shows the critical voltage needed to remove a 10 μm-radius droplet jumping upwards for a condensation heat flux of 0.5 W/cm^2, in the (a) cylindrical and (b) spherical cases for different inner radii and electrode spacings. The results show that for both cylindrical and spherical cases, as the spacing between the electrodes ($R_2 - R_1$) increases V_{crit} increases (Fig. 5), due to the decrease in the electric field strength E as $r \to R_2$ (Fig.6) where gravity still has to be overcome even as the vapor drag force decays. Furthermore, as the radius of the inner electrode is varied (Fig. 7), I observe an optimal geometry for which V_{crit} is minimized, which in turn can be explained by the interaction of the electrostatic force and the drag force as two decaying functions from the inner electrode to the outer electrode. As the spacing between electrodes is decreased, the spherical and cylindrical cases converge to the parallel plate case (see Appendix, Section A3) due to the similar radii of curvature between the inner and outer electrodes (analogous to a tube with large curvature being approximated by a flat plate). In the parallel plate limit, V_{crit} varies linearly with spacing. This suggests that the electrostatic term is dominant and inertia from the initial jumping velocity can be effectively neglected. Indeed, we can see from Fig. 2b that without an electric field, the jumping occurs over a few millimeters which makes the electrostatic force the dominant effect in getting the droplet to move distances on the order of centimeters. It is important to note that the critical voltage results shown here (Fig. 5) are orientation dependent (droplets jumping downwards would have different V_{crit} due to the reversal of gravitational force direction). However, these results (Fig. 5) act as upper limits for the required V_{crit} to successfully remove jumping droplets independent of jumping orientation.

3.3. Condensation Heat Flux

For high heat flux EFE applications such as electronics thermal management, the dominant force retarding jumping droplet motion away from the superhydrophobic surface will be the vapor drag force. According to Eqns. (2), (10) and (11), the magnitude of this force is both geometry and heat flux dependent. The vapor drag force increases linearly for the parallel plate case, while for the cylindrical and spherical cases, we would expect a non-linear effect of heat flux on drag due to the increasing cross-sectional area for vapor flow as we move away from the inner electrode (superhydrophobic surface). Figure 8 shows V_{crit} as a function of heat flux for droplets having R_{d} = 10 μm and jumping upward. The spacing between the electrodes was fixed at 2 cm and the inner radius was varied to investigate the effects of convergence between the two radii. The results show that V_{crit} increases as the heat flux increases for all geometries. In addition, the results show that with suitable electrode selection, V_{crit} and the total input power needed to maintain the electric field can be minimized. For the parallel case, a linear behavior appears for low Reynolds numbers (~0.1) due to the drag force being modeled as linear with velocity ($F_{\mathrm{D}} = 6\pi\mu_{\mathrm{v}}\left(u_{\mathrm{d,y}} + u_{\mathrm{v,y}}\right)R_{\mathrm{d}}$) which in turn is linear with heat flux according to Eq. (2). As for the cylindrical and spherical cases, the cylindrical geometry is advantageous at low heat fluxes ($q" < 2$ W/cm^2) while the spherical geometry is advantageous at larger heat fluxes ($q" > 2$ W/cm^2). It is important to note that from an application standpoint, the spherical geometry would not have much use in industrial settings due to the added difficulty of manufacture. The majority of condensation phase change applications utilize planar (vapor chambers) or cylindrical (industrial shell-and-tube steam condensers) geometries. Furthermore, the results shown here (Fig. 8) are

applicable for the particular chosen geometry and will vary with different EFE condenser designs.

3.4. Surface Orientation and Initial Jumping Position

Insofar, the results shown have utilized the conservative case of droplets jumping upward against gravity. To study the effect of surface orientation and jumping droplet position (in the non-planar geometries), the initial jumping position was varied in the model. The initial position affects the angle between the gravitational force facing downward and the electrostatic force acting in the radial direction. I simulated droplets with R_d = 10 μm for a heat flux of 0.5 W/cm^2 and for several applied voltages between the inner and outer electrode of a cylindrical geometry (Fig. 9). Below a critical voltage (≈ 45 V), some droplets return to the inner electrode and others make it to the outer electrode (Fig. 9a). For higher voltages (≈80-120 V) most of the droplets reach the outer electrode while the droplet jumping in the upward direction does not reach the outer electrode in the specified time constraint (Fig. 9b, c). Even at these voltages, the droplets' velocities are small when compared to velocities at higher voltages (≈220 V), where the droplets' trajectories are relatively straight (Fig. 9d). A quantitative measure of the effect of orientation is shown in Fig. 10, where depending on the magnitude of the electric field applied, a certain portion of the area of the condensing surface is effective (all droplet removed) while the rest will undergo progressive flooding that will impede heat transfer and render it ineffective as vapor continues to condense.

3.5. Efficiency of EFE Condensation

In order to maintain the electric field required for EFE condensation, a steady current must be supplied to the device in order to match the charge being deposited on the outer electrode from the jumping-droplets. At higher heat fluxes, the magnitude of the charge supplied and the required voltage can lead to high power consumption, making it important to define the efficiency of EFE condensation in terms of the power needed to maintain the critical electric fields. In order to give a quantitative measure of the efficiency, I define a parameter called the incremental coefficient of performance (COP_{inc}) as the ratio of the increase in heat flux due to EFE condensation to the electric input power needed:

$$COP_{\text{inc}} = \frac{q''_{\text{E}} - q''_{0}}{VI''}, \tag{21}$$

where q''_{E} and q''_{0} represent the heat flux (per unit area) with and without application of an external electric field, respectively, V represents the voltage applied for EFE condensation and I'' represents the current density due to the flow of positive charges (droplets). Note, the current density considered here occurs at steady state, and does not include the displacement current which occurs during initial transient charging of the electrodes by the power supply. The heat flux can be found by relating the mass of condensate per unit time per unit area ($\dot{m}''_{\text{cond}}$) to the latent heat of phase change (h_{fg}), $q'' = \dot{m}''_{\text{cond}} h_{\text{fg}}$.

Applying mass conservation for steady state at the surface, $\dot{m}''_{\text{cond}} = \dot{m}''_{\text{jump}}$, where $\dot{m}''_{\text{jump}}$ denotes the mass of jumping droplets per unit time per unit area. To

simplify the calculation, I assumed a constant jumping-droplet diameter of R_{d} = 10 μm. This assumption is valid given that the majority of jumping droplet events occur at length scales close to R_{d} = 10 μm. Realizing that $I'' = q_{\mathrm{d}}\dot{N}''_{\mathrm{jump}}$, where q_{d} is the charge of the droplet, and $\dot{N}''_{\mathrm{jump}}$ is given by Eq. (12), and combining Eqns. (12) and (21), I obtain:

$$COP_{\mathrm{inc}} = \frac{4\pi {R_d}^3 h_{\mathrm{fg}}\rho_{\mathrm{w}}}{3V q''_{\mathrm{E}} q_{\mathrm{d}}}\left(q''_{\mathrm{E}} - q''_{0}\right) \tag{22}$$

To obtain a realistic estimate for COP_{inc}, experimental conditions of a previous EFE condensation experimental study were used.[55] Values of q''_{E} and q''_{0} range between 0.1 to 0.8 W/cm^2 for log mean temperature differences ($LMTD$) between the vapor and cooling water ranging between 0.2 and 1°C,[55] respectively, and q_{d} ≈15 fC.[40] Figure 11 shows COP_{inc} as a function of $LMTD$. As the $LMTD$ increases, the heat flux increases, increasing the drag force on the jumping droplets. This will require a higher voltage for a given enhancement in heat transfer, and a lower COP_{inc}. Most importantly, the magnitude of COP_{inc} for these experiments is ~10^6 which proves that EFE condensation has a very high incremental efficiency. In fact, the high COP_{inc} can be generalized for different electrode geometries and supersaturation levels since it is governed by the heat transfer of individual droplets. To better understand the high magnitude of COP_{inc}, I analyze the physical mechanism of droplet removal in an electric field. By removing a droplet that would have otherwise returned to the superhydrophobic surface without the electric field, I allow another droplet of the same size to form in its place and hence add an extra heat transfer $dq = mh_{\mathrm{fg}}$. The work needed to remove the droplet is $dw = q_{\mathrm{d}}V$, where V is the applied voltage between the electrodes. The COP_{inc} can now be estimated as $COP_{\mathrm{inc}} \sim dq/dw \sim$ 2x10^6, where R_{d} ~ 10 μm, ρ_{w} ~ 992 kg/m^3, h_{fg} ~ 2.4 MJ/kg, q_{d} ~ 15

fC, and V ~ 300 V. This scaling analysis assumes that returning droplets inhibit heat transfer and do not undergo further growth, which is deemed as a valid approximation given the severely reduced droplet growth rate of larger droplets on superhydrophobic surfaces due to heat conduction resistance through the droplet body and base.

It is important to note that very high COP_{inc} (~10^6) does not mean that the overall *COP* of the system is very high. Rather, it indicates that any added heat transfer enhancement due to the use of external electric fields far outweigh the drawbacks of providing the electrical power to maintain those fields. For this particular experimental case, the overall system COP is enhanced by ≈50% when compared to non-EFE jumping-droplet condensation, making EFE condensation highly attractive from an energetic standpoint.

3.6. Condensate Removal

One main challenge that accompanies the innovation provided by EFE condensation is the removal of the liquid from the outer electrode. As the droplets are attracted to the negatively charged electrode, they will deposit on the electrode and reside there until a large enough liquid layer builds up for gravitational removal, or slowly evaporate depending on the temperature of the electrode. Liquid buildup on the electrode can pose potential problems for EFE condensation depending on the voltage of the system. If the voltage difference between electrodes is large enough and liquid bridging occurs, electrolysis can initiate and unwanted production of hydrogen (a non-condensable gas) inside the condenser will ensue. Furthermore, depending on the gap spacing between the electrodes, liquid can potentially bridge the gap and inundate the superhydrophobic

surface with condensate if not properly removed from the outer electrode. One potential method of eliminating liquid buildup on the outer electrode would be to design the electrodes to be porous and superhydrophilic.[71-72] By doing so, the electrode can collect the attracted water droplets and pump them away from the condenser *via* capillary pressure.[73] However this mechanism would incorporate challenges such as having to eventually evaporate the liquid in order to maintain the capillary pressure inside the wicking structure. Furthermore, the capillary pumping mechanism may not be fast enough to remove all accumulated condensate during high heat flux operation, when droplets accumulate at a higher rate.

A second and highly desirable condensate removal mechanism involves the careful design of split electrodes that naturally allow for the motion of water droplets past the outer electrode without loss of functionality. To demonstrate this concept, I utilized my developed model to show the trajectory of departing droplets for a radial tube configuration (Fig. 3a) having a gap in the outer electrode at the bottom. By properly specifying the voltage applied to the electrodes, droplet can be effectively removed below both tubes with minimal droplet return (Fig. 12a). To verify the robustness of this approach, I also calculated the droplet trajectory for a range of droplet sizes with similar results (Fig. 12b), indicating that geometric and electrostatic considerations can be used to enable successful long term EFE condensation operation. It is important to note, droplets at the very top of the radial condensing surface cannot be collected at the bottom if their initial velocity is normal to the surface (jumping upwards). If droplet jumping does not occur again upon droplet return, progressive flooding may initiate at the top surface. This risk is mitigated by the fact that the probability of having an upward

trajectory at the top surface tends to zero since most droplets jump at some angle away from the surface[12, 21] and the area having a surface normal in the upward direction is infinitesimally small for a radial geometry.

Although my model has demonstrated that EFE condensation can be used for effective condensate removal, future investigations of EFE droplet motion in bulk advective vapor flow conditions are needed given the variety or applications utilizing flow condensation such as heat pipes and internal condensers. Although my results present a promising approach to delay progressive flooding, more work is needed to extend the range of nucleation mediated flooding which currently has been experimentally shown to occur at supersaturations $S < 1.12$ and heat fluxes $q'' < 8$ W/cm^2 for silane coated CuO superhydrophobic surfaces.[17] The quantification of droplet size distribution during steady-state jumping droplet condensation for different supersaturations is also needed to elucidate the inter-droplet spacing as currently used approximations (square array), derived for non-interacting droplets in dropwise condensation, may not be valid for jumping-droplet condensers. Furthermore, it would be interesting to expand the developed model to incorporate many-droplet systems such that Coulombic interactions between multiple jumping droplets can be investigated and optimized for maximizing heat transfer and condensate mitigation. In addition, it would be interesting to investigate electrowetting effects at high voltages and small electrode spacings to determine critical field strength values for which jumping no longer occurs. Although not considered here due to the relatively large spacing between the droplets and the condensing surface (where the electric field can be approximated as the solution

between two smooth electrodes), it would be interesting to investigate the effects of rough electrodes (such as the rough CuO used here) on electric field strength and non-uniformity close to the superhydrophobic surface, and how it affects droplet motion[74]. Lastly, it would be worthwhile to utilize the developed model to study jumping-droplet electrostatic energy harvesting,[39] and perform further optimization for power generation performance.

3.7. Figures

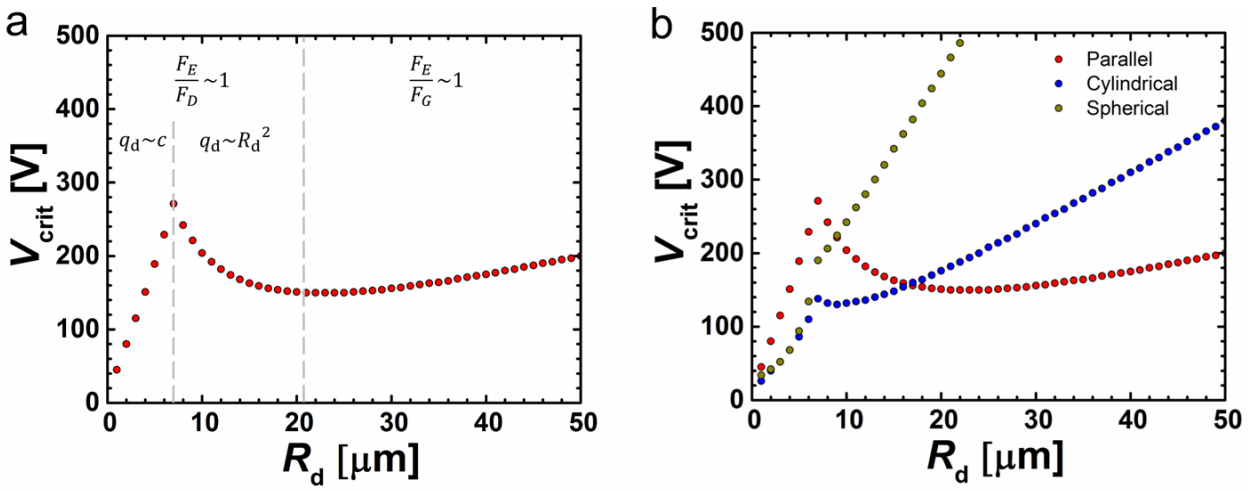

Figure 4. Critical voltage (V_{crit}) needed to remove a droplet of radius R_{d} completely (the droplet reaches the outer electrode) for a range of droplet sizes ($1\mu m \leq R_{\mathrm{d}} \leq 50\mu m$). The model represents droplet jumping in the upward direction (against gravity). (a) Droplet is jumping from a flat plate (parallel plate capacitor case). We observe different regimes under which the behavior of the curve differs. For low radii ($R_{\mathrm{d}} < 20\mu m$) , drag force F_D dominates hence the electrostatic force F_E should balance the vapor drag (F_E/F_D~1). Within this range, we distinguish two different regimes depending on the charge of the droplet: $q_{\mathrm{d}} = 10$ fC for $R_{\mathrm{d}} < 7$ μm and $q_{\mathrm{d}} = 17e^{-6}(4\pi {R_{\mathrm{d}}}^2)$, where q_{d} is in Coulombs and R_{d} is in meters, for $R_{\mathrm{d}} > 7$ μm.[55]

For larger radii ($R_{\mathrm{d}} > 20\mu m$), the gravitational force F_G dominates which needs to be counteracted by the electrostatic force ($F_E/F_G \sim 1$). (b) Comparison of three different geometries of condensing surface: flat plate, cylindrical tube (cylindrical capacitor case) and spherical ball (spherical capacitor case). Inner and outer radii of the electrodes are, respectively, R_1 = 3 mm and R_2 = 2 cm, whereas in the case of parallel plates the spacing considered is $R_2 - R_1$. Heat flux considered is q" = 0.5 W/cm^2.

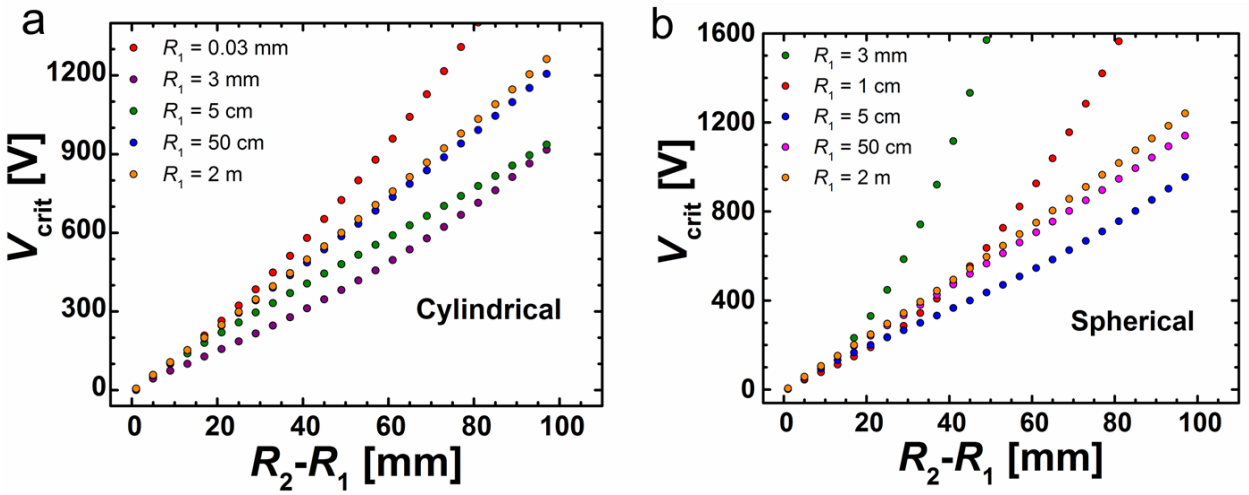

Figure 5. Critical voltage needed to remove a droplet of R_{d} = 10 μm completely (the droplet reaches the outer electrode). The droplet jumps from a (a) cylindrical superhydrophobic surface and (b) spherical superhydrophobic surface**.** The inner and outer electrodes have radii of R_1 and R_2, respectively. The heat flux considered is 0.5 W/cm^2. For large R_1, both the cylindrical and spherical geometries converge to the parallel plate capacitor case, where the critical voltage is linear with electrode spacing. The curves also show that there is an optimal geometry for which V_{crit} is minimal.

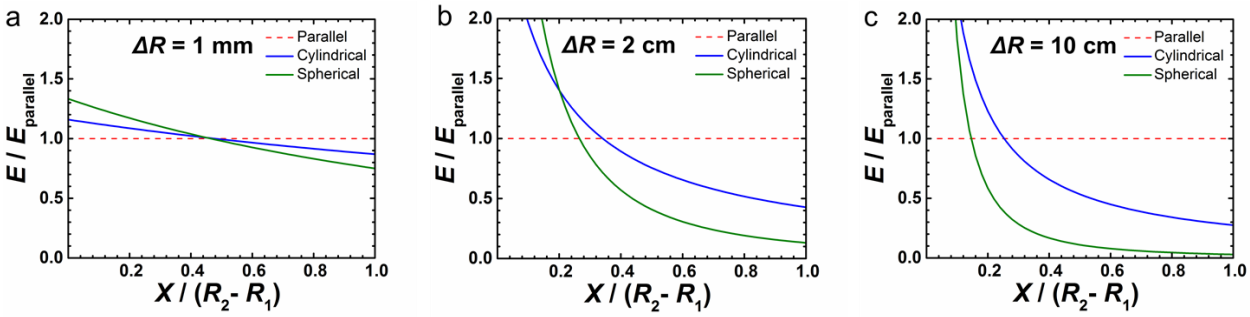

Figure 6. Normalized electric field amplitude (E/E_{parallel}) in terms of the distance (X) from inner electrode normalized by the distance between the two electrodes ($R_2 - R_1$). The electric field amplitude of the cylindrical and spherical capacitors is plotted for an inner radius R_1 = 3 mm and for several electrode spacings. (a) $\Delta R = R_2 - R_1$ = 1 mm. (b) ΔR = 2 cm. (c) ΔR = 10 cm. High ΔR reflects high non linearity in the electric field distribution along radial positions from the center of the electrodes and low ΔR reflects a parallel plate capacitor case, for both cylindrical and spherical capacitors. The optimal geometry for droplet removal corresponds to some intermediate values of ΔR, for a fixed R_1.

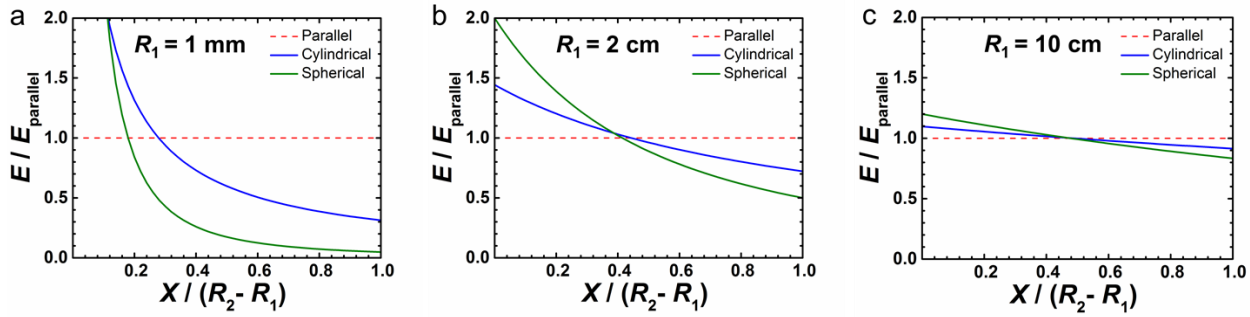

Figure 7. Normalized electric field amplitude ($E/E_{parallel}$) in terms of the distance (X) from inner electrode normalized by the distance between the two electrodes ($R_2 - R_1$). The electric field amplitude of the cylindrical and spherical capacitors is plotted for a spacing of $R_2 - R_1$ = 2

cm and for several inner radii. (a) $R_1 = 1$ mm. (b) $R_1 = 2$ cm. (c) $R_1 = 10$ cm. Small R_1 reflects high non linearity in the electric field distribution along radial positions from the center of the electrodes and high R_1 reflects a parallel plate capacitor case, for both cylindrical and spherical capacitors. The optimal geometry for droplet removal corresponds to some intermediate values of R_1, for a fixed ΔR.

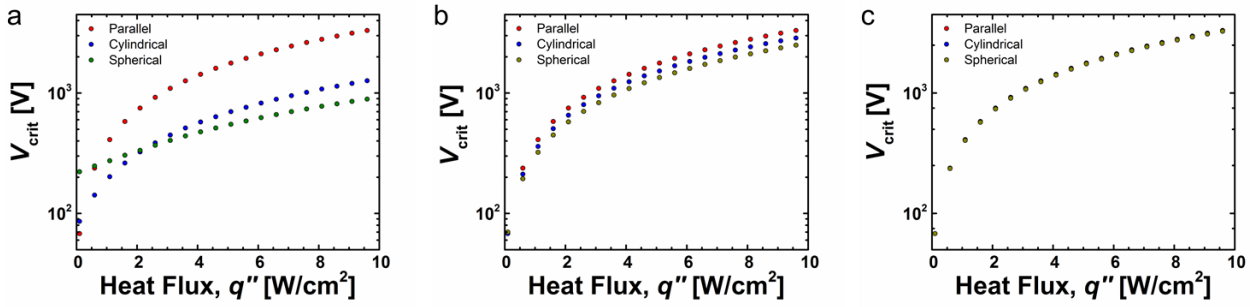

Figure 8. Heat flux effect on the critical voltage (V_{crit}) needed to remove a droplet of radius 10 μm. The inner radii R_1 of the spherical and cylindrical surfaces are varied to validate the parallel plate limit at large R_1. (a) R_1 = 3 mm. (b) R_1 = 50 mm. (c) R_1 = 1 m. The spacing between the electrodes is considered to be 2 cm. An increasing heat flux would result in a higher V_{crit} for all geometries. However, a suitable design of the electrodes can minimize that effect and hence minimize the input power needed. This is illustrated by the more gentle slopes for spherical and cylindrical geometries in (a).

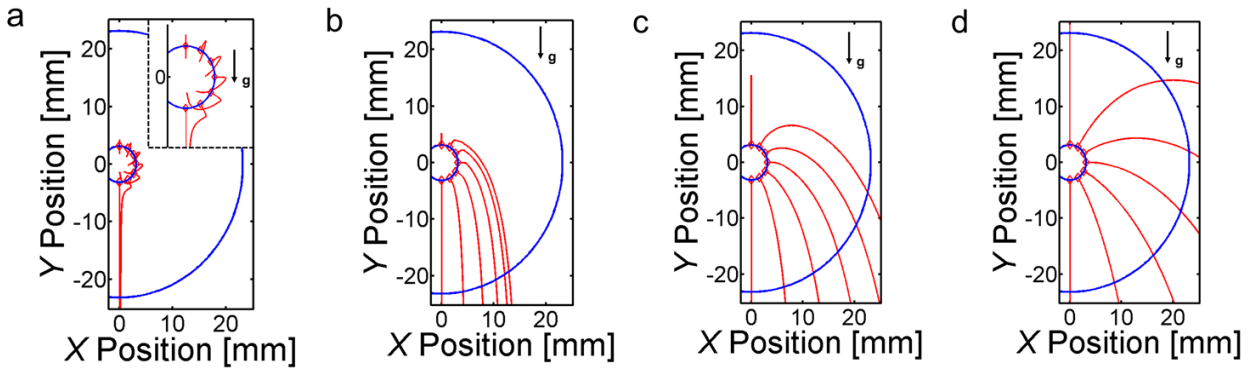

Figure 9. Trajectories of droplets jumping from a cylindrical SPF coated superhydrophobic surface, subjected to an external electric field established by a voltage difference between the inner and outer electrodes (the inner electrode being charged positively) for (a) 45 V, (b) 80 V, (c) 120 V, and (d) 220 V. The droplets considered have radii of 10 μm, the heat flux considered is 0.5 W/cm^2, and the inner and outer radii of the electrodes are fixed at 3 mm and 23 mm, respectively. The initial position of each droplet is marked by a hollow rhombus. The results clearly show that a threshold voltage exists that is able to remove all jumping droplets from the condensing tube.

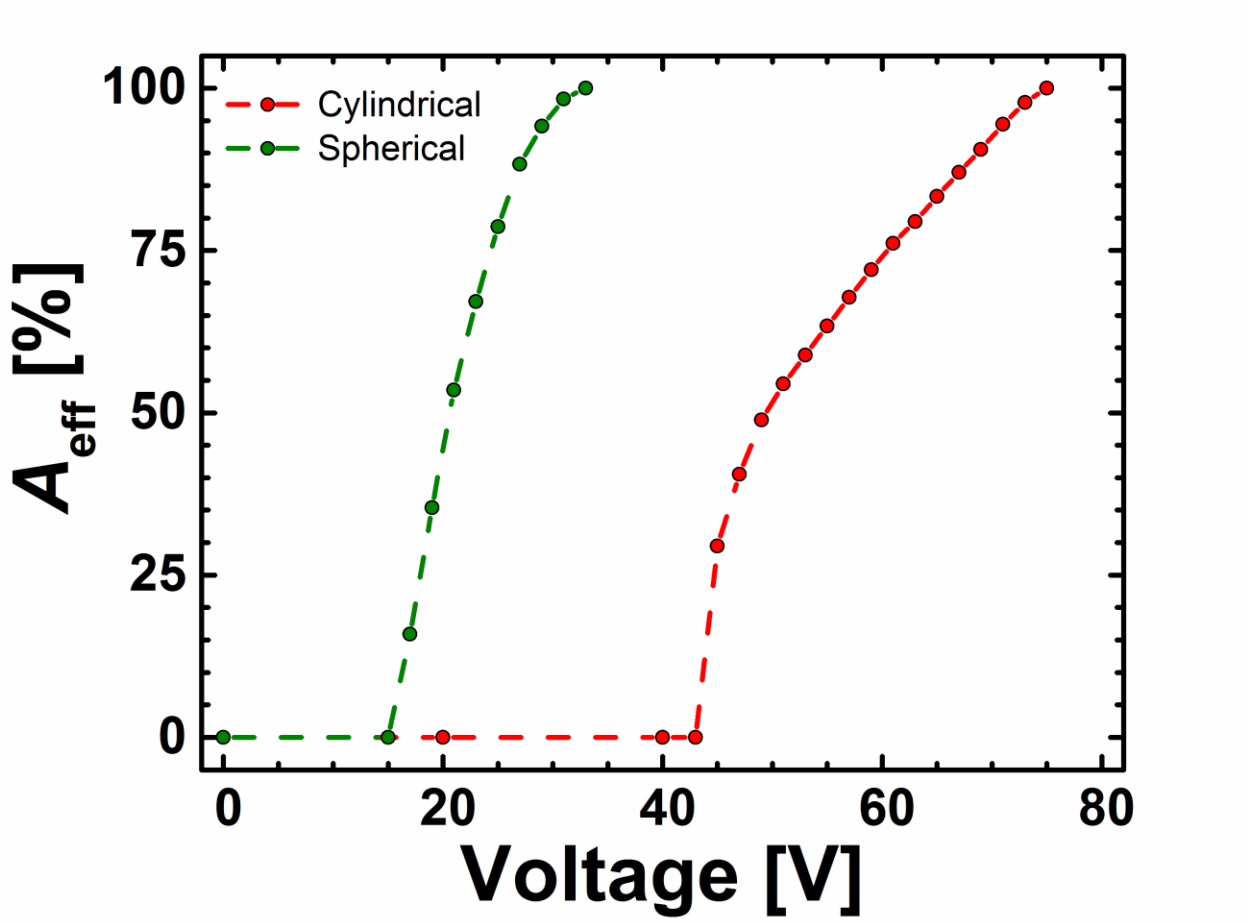

Figure 10. Effective surface area (A_{eff}) in terms of the voltage applied between the electrodes for a cylindrical and spherical condensing surface. The effective area represents the fraction (in percentage) of the area of the condensing surface where droplets are being removed under the effect of the external electric field, that is, where heat transfer is enhanced. This is a quantitative measure of the effect of the initial position of the droplet, meaning the direction of its initial velocity (Fig. 9). The droplets are considered to have a radius of 10 μm, the inner and outer electrodes are considered of 3 mm and 2 cm radii, respectively, and the heat flux considered is 0.5 W/cm^2.

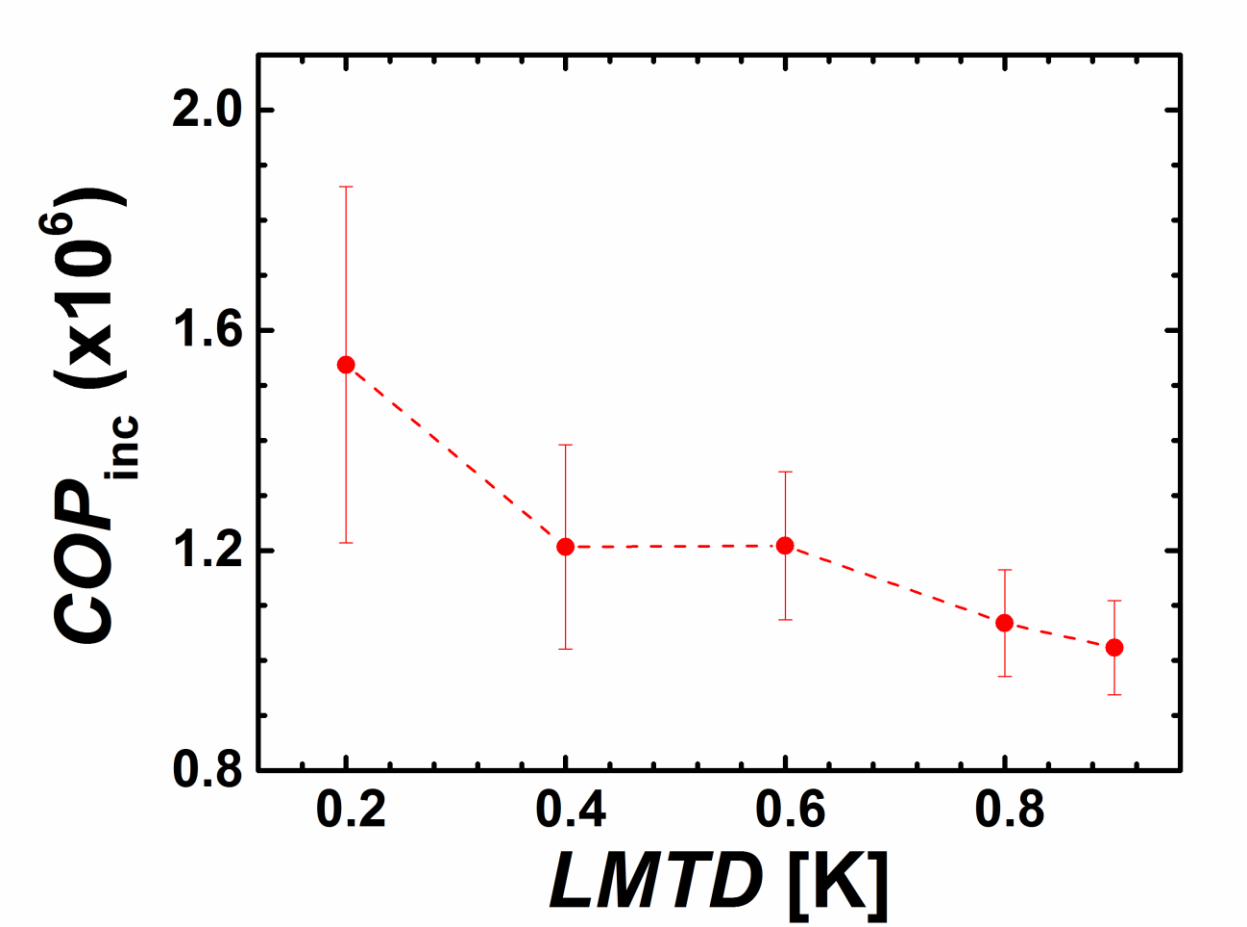

Figure 11. Incremental COP (COP_{inc}) of the electric field enhanced (EFE) condensation in terms of the logarithmic mean temperature difference (*LMTD*) between the hot vapor and the condensing surface. COP_{inc} is defined as the ratio of the heat transfer enhancement to electric power input, and is given by Eq. (22). The increased heat transfer ranges between 0.1 to 0.8 W/cm^2 in experimental measurements.[55] The electric power input is found from the critical voltage needed to remove a droplet of 10 μm radius jumping from a SPF coated superhydrophobic flat surface (V ~ 200 V). The error bars were calculated with propagation of error from the experimental uncertainties associated with the experimental measurements[55] of q''_E and q''_0, assuming negligible error on the other parameters in Eq. 22.

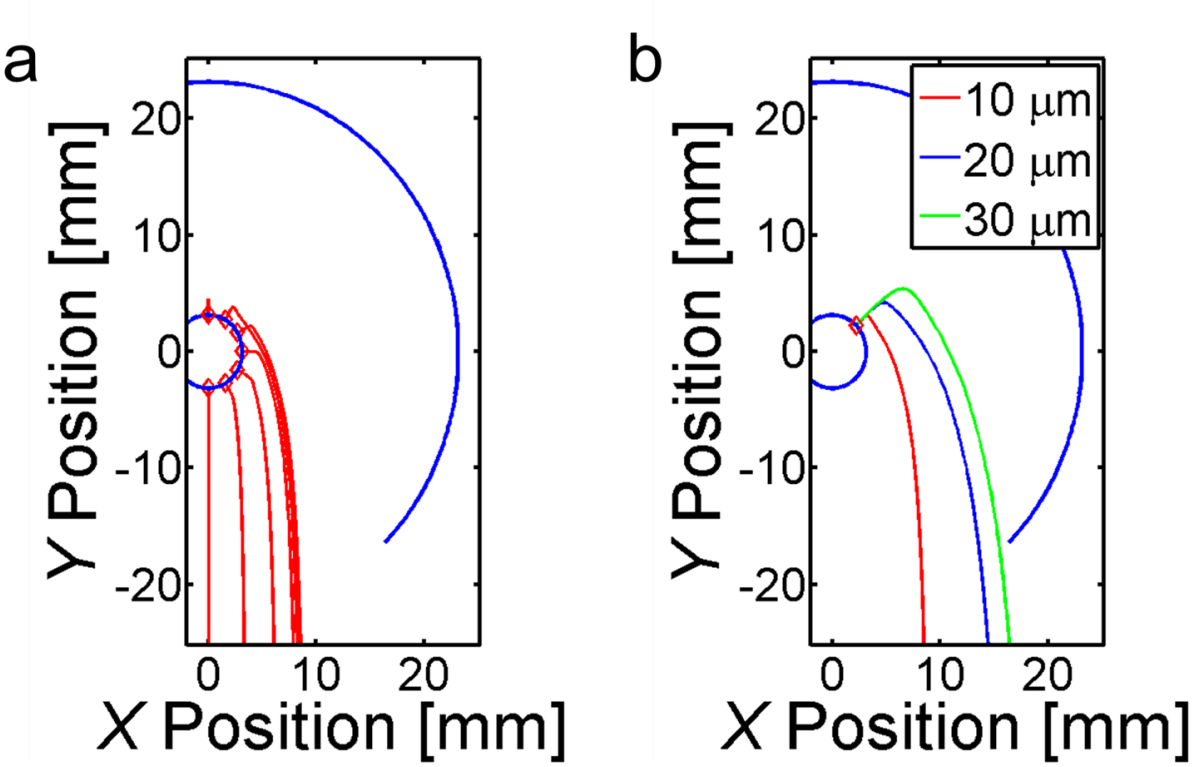

Figure 12. Proper application of external electric field for droplet collection at the bottom of the cylindrical outer electrode. The heat flux considered is 0.5 W/cm^2 and. (a) Droplets of 10 μm radius departing from different locations on the condensing electrode. Inner and outer radii of electrodes are 3 mm and 2 cm, respectively. Voltage applied is 70 V. (b) Droplets of 10, 20 and 30 μm radius departing from same location on the condensing electrode. Inner and outer radii of electrodes are 3 mm and 2.3 cm, respectively. The voltage applied is 60 V.

CHAPTER 4: CONCLUSIONS

I have developed a comprehensive physical model to predict the performance and efficiency of the electric-field-enhanced jumping-droplet condensation on nanostructured superhydrophobic surfaces under a variety of different conditions. I first validated the simple jumping droplet model (without EFE condensation) by comparing the theoretical trajectories of droplets to real high speed experimental data, with excellent agreement. Then, by incorporating the contribution of an externally applied voltage between the condensing surface and an outer electrode while considering the effects of droplet size, electrodes size and geometry, condensation heat flux, and droplet jumping direction, I showed that smaller jumping droplets and smaller heat fluxes require less work input to be removed. Using my model, I then showed that the electrodes can be designed such that the work input is minimized, and determined the effective portion of condensing surface for a given external voltage due to orientation effects. By defining an incremental coefficient of performance that describes the efficiency of the EFE condensation, I showed the incremental COP to be very large ($\sim 10^6$) indicating that the added energy required to create electric fields for EFE condensation is negligible when compared to the added benefit of heat transfer enhancement. Subsequently, the model was used to study geometric electrode designs for condensate mitigation and collection, showing that radial configurations with slotted gaps are potentially highly advantageous designs. The findings have significant relevance to the applications of EFE condensation for efficient phase change heat transfer applications.

REFERENCES

1. Rose, J. W. Dropwise condensation theory and experiment: a review. *P I Mech Eng a-J Pow* **2002,** *216* (A2), 115-128.
2. Schmidt, E.; Schurig, W.; Sellschopp, W. Versuche über die Kondensation von Wasserdampf in Film- und Tropfenform. *Forsch. Ingenieurwes* **1930,** *1* (2), 53–63.
3. Le Fevre, E. J.; Rose, J. W. Heat-Transfer Measurements During Dropwise Condensation of Steam. *International Journal of Heat and Mass Transfer* **1964,** *7*, 272-273.
4. Le Fevre, E. J.; Rose, J. W. In *A Theory af Heat Transfer by Dropwise Condensation*, Proceedings of the Third International Heat Transfer Conference, Chicago, IL, 1966; ASME, pp 362-375.
5. McCormick, J. L.; Baer, E. On Mechanism of Heat Transfer in Dropwise Condensation. *J Coll Sci Imp U Tok* **1963,** *18* (3), 208-216.
6. Mikic, B. B. On Mechanism of Dropwise Condensation. *International Journal of Heat and Mass Transfer* **1969,** *12*, 1311-1323.
7. Tanner, D. W.; Pope, D.; Potter, C. J.; West, D. Heat Transfer in Dropwise Condensation. *International Journal of Heat and Mass Transfer* **1965,** *8*, 427-436.
8. Umur, A.; Griffith, P. Mechanism of Dropwise Condensation. *J Heat Transf* **1965,** *87* (2), 275–282.
9. Wu, W. H.; Maa, J. R. On the Heat Transfer in Dropwise Condensation. *Chemical Engineering Journal* **1976,** *12* (3), 225–231.
10. Kim, S.; Kim, K. J. Dropwise Condensation Modeling Suitable for Superhydrophobic Surfaces. *J Heat Transf* **2011,** *133* (8), 081502.
11. Boreyko, J. B.; Chen, C. H. Self-Propelled Dropwise Condensate on Superhydrophobic Surfaces. *Phys Rev Lett* **2009,** *103* (18), 184501.
12. Enright, R.; Miljkovic, N.; Sprittles, J.; Nolan, K.; Mitchell, R.; Wang, E. N. How Coalescing Droplets Jump. *ACS Nano* **2014,** *8* (10), 10352-10362.
13. Liu, F. J.; Ghigliotti, G.; Feng, J. J.; Chen, C. H. Numerical simulations of self-propelled jumping upon drop coalescence on non-wetting surfaces. *J Fluid Mech* **2014,** *752*, 39-65.
14. Liu, F. J.; Ghigliotti, G.; Feng, J. J.; Chen, C. H. Self-propelled jumping upon drop coalescence on Leidenfrost surfaces. *J Fluid Mech* **2014,** *752*, 22-38.
15. Nam, Y.; Kim, H.; Shin, S. Energy and hydrodynamic analyses of coalescence-induced jumping droplets. *Appl Phys Lett* **2013,** *103* (16).
16. Nam, Y.; Seo, D.; Lee, C.; Shin, S. Droplet coalescence on water repellant surfaces. *Soft Matter* **2015,** *11* (1), 154-160.
17. Miljkovic, N.; Enright, R.; Nam, Y.; Lopez, K.; Dou, N.; Sack, J.; Wang, E. N. Jumping-Droplet-Enhanced Condensation on Scalable Superhydrophobic Nanostructured Surfaces. *Nano Letters* **2013,** *13* (1), 179-187.
18. Chen, X.; Wu, J.; Ma, R.; Hua, M.; Koratkar, N.; Yao, S.; Wang, Z. Nanograssed Micropyramidal Architectures for Continuous Dropwise Condensation. *Advanced Functional Materials* **2011,** *21*, 4617–4623.
19. Feng, J.; Pang, Y.; Qin, Z.; Ma, R.; Yao, S. Why Condensate Drops Can Spontaneously Move Away on Some Superhydrophobic Surfaces but Not on Others. *ACS Applied Materials & Interfaces* **2012,** *4*, 6618−6625.
20. Feng, J.; Qin, Z. Q.; Yao, S. H. Factors Affecting the Spontaneous Motion of Condensate Drops on Superhydrophobic Copper Surfaces. *Langmuir* **2012,** *28* (14), 6067-6075.

21. Lv, C. J.; Hao, P. F.; Yao, Z. H.; Song, Y.; Zhang, X. W.; He, F. Condensation and jumping relay of droplets on lotus leaf. *Appl Phys Lett* **2013,** *103*, 021601.
22. Rykaczewski, K. Microdroplet Growth Mechanism during Water Condensation on Superhydrophobic Surfaces. *Langmuir* **2012,** *28* (20), 7720-7729.
23. Rykaczewski, K.; Osborn, W. A.; Chinn, J.; Walker, M. L.; Scott, J. H. J.; Jones, W.; Hao, C.; Yaod, S.; Wang, Z. How nanorough is rough enough to make a surface superhydrophobic during water condensation? *Soft Matter* **2012,** *8*, 8786-8794.
24. Tian, J.; Zhu, J.; Guo, H. Y.; Li, J.; Feng, X. Q.; Gao, X. F. Efficient Self-Propelling of Small-Scale Condensed Microdrops by Closely Packed ZnO Nanoneedles. *J Phys Chem Lett* **2014,** *5* (12), 2084-2088.
25. McCarthy, M.; Gerasopoulos, K.; Maroo, S. C.; Hart, A. J. Materials, Fabrication, and Manufacturing of Micro/Nanostructured Surfaces for Phase-Change Heat Transfer Enhancement. *Nanosc Microsc Therm* **2014,** *18* (3), 288-310.
26. Li, G. Q.; Alhosani, M. H.; Yuan, S. J.; Liu, H. R.; Al Ghaferi, A.; Zhang, T. J. Microscopic Droplet Formation and Energy Transport Analysis of Condensation on Scalable Superhydrophobic Nanostructured Copper Oxide Surfaces. *Langmuir* **2014,** *30* (48), 14498-14511.
27. Yanagisawa, K.; Sakai, M.; Isobe, T.; Matsushita, S.; Nakajima, A. Investigation of droplet jumping on superhydrophobic coatings during dew condensation by the observation from two directions. *Appl Surf Sci* **2014,** *315*, 212-221.
28. Lo, C. W.; Wang, C. C.; Lu, M. C. Scale Effect on Dropwise Condensation on Superhydrophobic Surfaces. *ACS Applied Materials & Interfaces* **2014,** *6* (16), 14353-14359.
29. Wisdom, K. M.; Watson, J. A.; Qua, X.; Liua, F.; Watson, G. S.; Chen, C. H. Self-cleaning of superhydrophobic surfaces by self-propelled jumping condensate. *Proceedings of the National Academy of Sciences of the United States of America* **2013,** *110* (20), 7992–7997.
30. Watson, G. S.; Schwarzkopf, L.; Cribb, B. W.; Myhra, S.; Gellender, M.; Watson, J. A. Removal mechanisms of dew via self-propulsion off the gecko skin. *J R Soc Interface* **2015,** *12* (105).
31. Watson, G. S.; Gellender, M.; Watson, J. A. Self-propulsion of dew drops on lotus leaves: a potential mechanism for self cleaning. *Biofouling* **2014,** *30* (4), 427-434.
32. Boreyko, J. B.; Zhao, Y. J.; Chen, C. H. Planar jumping-drop thermal diodes. *Appl Phys Lett* **2011,** *99* (23), 234105.
33. Boreyko, J. B.; Collier, P. C. Delayed Frost Growth on Jumping-Drop Superhydrophobic Surfaces. *Acs Nano* **2013,** *7* (2), 1618-1627.
34. Chen, X. M.; Ma, R. Y.; Zhou, H. B.; Zhou, X. F.; Che, L. F.; Yao, S. H.; Wang, Z. K. Activating the Microscale Edge Effect in a Hierarchical Surface for Frosting Suppression and Defrosting Promotion. *Sci Rep-Uk* **2013,** *3*.
35. Lv, J. Y.; Song, Y. L.; Jiang, L.; Wang, J. J. Bio-Inspired Strategies for Anti-Icing. *ACS Nano* **2014,** *8* (4), 3152-3169.
36. Zhang, Q. L.; He, M.; Chen, J.; Wang, J. J.; Song, Y. L.; Jiang, L. Anti-icing surfaces based on enhanced self-propelled jumping of condensed water microdroplets. *Chem Commun* **2013,** *49* (40), 4516-4518.
37. Boreyko, J. B.; Chen, C. H. Vapor chambers with jumping-drop liquid return from superhydrophobic condensers. *International Journal of Heat and Mass Transfer* **2013,** *61*, 409-418.

38. Preston, D. J.; Miljkovic, N.; Enright, R.; Wang, E. N. Jumping Droplet Electrostatic Charging and Effect on Vapor Drag. *J Heat Trans-T Asme* **2014,** *136* (8).
39. Miljkovic, N.; Preston, D. J.; Enright, R.; Wang, E. N. Jumping-droplet electrostatic energy harvesting. *Appl Phys Lett* **2014,** *105* (1).
40. Miljkovic, N.; Preston, D. J.; Enright, R.; Wang, E. N. Electrostatic charging of jumping droplets. *Nat Commun* **2013,** *4*.
41. Enright, R.; Miljkovic, N.; Alvarado, J. L.; Kim, K.; Rose, J. W. Dropwise Condensation on Micro- and Nanostructured Surfaces. *Nanosc Microsc Therm* **2014,** *18* (3), 223-250.
42. Miljkovic, N.; Wang, E. N. Condensation heat transfer on superhydrophobic surfaces. *Mrs Bull* **2013,** *38* (5), 397-406.
43. Enright, R.; Miljkovic, N.; Dou, N.; Nam, Y.; Wang, E. N. Condensation on Superhydrophobic Copper Oxide Nanostructures. *J Heat Transf* **2013,** *135* (9), 091304.
44. Miljkovic, N.; Enright, R.; Wang, E. N. Effect of Droplet Morphology on Growth Dynamics and Heat Transfer during Condensation on Superhydrophobic Nanostructured Surfaces. *Acs Nano* **2012,** *6* (2), 1776–1785.
45. Miljkovic, N.; Enright, R.; Wang, E. N. Growth Dynamics During Dropwise Condensation on Nanostructured Superhydrophobic Surfaces. *3rd Micro/Nanoscale Heat & Mass Transfer International Conference* **2012**.
46. Miljkovic, N.; Enright, R.; Wang, E. N. Modeling and Optimization of Condensation Heat Transfer on Micro and Nanostructured Superhydrophobic Surfaces. *J Heat Transf* **2013**, doi: 10.1115/1.4024597.
47. Cheng, J.; Vandadi, A.; Chen, C. L. Condensation heat transfer on two-tier superhydrophobic surfaces. *Appl Phys Lett* **2012,** *101*, 131909-1 - 131909-4.
48. Olceroglu, E.; Hsieh, C. Y.; Rahman, M. M.; Lau, K. K. S.; McCarthy, M. Full-Field Dynamic Characterization of Superhydrophobic Condensation on Biotemplated Nanostructured Surfaces. *Langmuir* **2014,** *30* (25), 7556-7566.
49. Olceroglu, E.; King, S. M.; Rahman, M. M.; McCarthy, M. Biotemplated Superhydrophobic Surfaces for Enhanced Dropwise Condensation. *Proceedings of the Asme International Mechanical Engineering Congress and Exposition - 2012, Vol 7, Pts a-D* **2013**, 2809-2815.
50. Attinger, D.; Frankiewicz, C.; Betz, A. R.; Schutzius, T. M.; Ganguly, R.; Das, A.; Kim, C.-J.; Megaridis, C. M. Surface engineering for phase change heat transfer: A review. *MRS Energy & Sustainability* **2014,** *1*.
51. Chen, X. M.; Weibel, J. A.; Garimella, S. V. Exploiting Microscale Roughness on Hierarchical Superhydrophobic Copper Surfaces for Enhanced Dropwise Condensation. *Adv Mater Interfaces* **2015,** *2* (3).
52. Hou, Y. M.; Yu, M.; Chen, X. M.; Wang, Z. K.; Yao, S. H. Recurrent Filmwise and Dropwise Condensation on a Beetle Mimetic Surface. *ACS Nano* **2015,** *9* (1), 71-81.
53. Lv, C. J.; Hao, P. F.; Yao, Z. H.; Niu, F. L. Departure of Condensation Droplets on Superhydrophobic Surfaces. *Langmuir* **2015,** *31* (8), 2414-2420.
54. Rykaczewski, K.; Paxson, A. T.; Anand, S.; Chen, X.; Wang, Z.; Varanasi, K. K. Multimode Multidrop Serial Coalescence Effects during Condensation on Hierarchical Superhydrophobic Surfaces. *Langmuir* **2013,** *29* (3), 881–891.
55. Miljkovic, N.; Preston, D. J.; Enright, R.; Wang, E. N. Electric-Field-Enhanced Condensation on Superhydrophobic Nanostructured Surfaces. *ACS Nano* **2013,** *7* (12), 11043-11054.

56. Enright, R.; Miljkovic, N.; Al-Obeidi, A.; Thompson, C. V.; Wang, E. N. Condensation on Superhydrophobic Surfaces: The Role of Local Energy Barriers and Structure Length Scale. *Langmuir* **2012,** *28* (40), 14424-14432.
57. Varanasi, K. K.; Deng, T. Controlling Condensation of Water Using Hybrid Hydrophobic-Hydrophilic Surfaces. *Proceedings of the Asme International Heat Transfer Conference - 2010, Vol 1* **2010**, 447-452.
58. Varanasi, K. K.; Hsu, M.; Bhate, N.; Yang, W. S.; Deng, T. Spatial control in the heterogeneous nucleation of water. *Appl Phys Lett* **2009,** *95* (9).
59. Mishchenko, L.; Khan, M.; Aizenberg, J.; Hatton, B. D. Spatial Control of Condensation and Freezing on Superhydrophobic Surfaces with Hydrophilic Patches. *Advanced Functional Materials* **2013,** *23* (36), 4577-4584.
60. Yamada, Y.; Ikuta, T.; Nishiyama, T.; Takahashi, K.; Takata, Y. Droplet Nucleation on a Well-Defined Hydrophilic-Hydrophobic Surface of 10 nm Order Resolution. *Langmuir* **2014,** *30* (48), 14532-14537.
61. Happel, J.; Brenner, H. *Low Reynolds number hydrodynamics : with special applications to particulate media*; 1st pbk. ed.; M. Nijhoff ;

Distributed by Kluwer Boston: The Hague ; Boston

Hingham, MA, USA, 1983. p 553 p.
62. White, F. M. *Fluid mechanics*; 6th ed.; McGraw-Hill: New York, 2008. p xiii, 864 p. ill.
63. Stone, H. A. Dynamics of Drop Deformation and Breakup in Viscous Fluids. *Annu Rev Fluid Mech* **1994,** *26*, 65-102.
64. Bertrand, C. L. *Electrostatics : theory and applications*; Nova Science Publishers: New York, 2011. p xi, 332 p.
65. He, M.; Zhang, Q. L.; Zeng, X. P.; Cui, D. P.; Chen, J.; Li, H. L.; Wang, J. J.; Song, Y. L. Hierarchical Porous Surface for Efficiently Controlling Microdroplets' Self-Removal. *Adv Mater* **2013,** *25* (16), 2291-2295.
66. Xiaopeng Qu, J. B. B., Fangjie Liu, Rebecca L. Agapov, Nickolay V. Lavrik, Scott T. Retterer, James J. Feng, Patrick Collier, and Chuan-Hua Chen. Self-propelled sweeping removal of dropwise condensate. *Appl Phys Lett* **2015,** *106* (221601).
67. Paulsen, J. D.; Burton, J. C.; Nagel, S. R.; Appathurai, S.; Harris, M. T.; Basaran, O. A. The inexorable resistance of inertia determines the initial regime of drop coalescence. *Proceedings of the National Academy of Sciences of the United States of America* **2012,** *109* (18), 6857-6861.
68. Eggers, J.; Lister, J. R.; Stone, H. A. Coalescence of liquid drops. *J Fluid Mech* **1999,** *401*, 293-310.
69. Paulsen, J. D.; Burton, J. C.; Nagel, S. R. Viscous to Inertial Crossover in Liquid Drop Coalescence. *Phys Rev Lett* **2011,** *106* (11), 114501.
70. Wu, M. M.; Cubaud, T.; Ho, C. M. Scaling law in liquid drop coalescence driven by surface tension. *Phys Fluids* **2004,** *16* (7), 51-54.
71. Gao, S. Y.; Jia, X. X.; Yang, J. M.; Wei, X. J. Hierarchically micro/nanostructured porous metallic copper: Convenient growth and superhydrophilic and catalytic performance. *J Mater Chem* **2012,** *22* (40), 21733-21739.
72. Huang, W. X.; Deng, W.; Lei, M.; Huang, H. Superhydrophilic porous TiO2 film prepared by phase separation through two stabilizers. *Appl Surf Sci* **2011,** *257* (11), 4774-4780.

73. Faghri, A. *Heat pipe science and technology*; Taylor & Francis: Washington, DC, 1995. p xxxiii, 874 p.
74. Zhao, Y. P.; Wang, G. C.; Lu, T. M.; Palasantzas, G.; De Hosson, J. T. M. Surface-roughness effect on capacitance and leakage current of an insulating film. *Phys Rev B* **1999,** *60* (12), 9157-9164.

APPENDIX

A.1. Electrowetting on Dielectric (EWOD) Model

The EWOD model[1] predicts that the contact angle of a droplet would be altered if the droplet is subjected to an electric field, by the following formula:

$$\cos\theta' = \cos\theta + \frac{\epsilon_0 \epsilon_{\mathrm{d}}}{2 d \sigma_{\mathrm{lv}}} V^2, \tag{A1}$$

where θ' and θ represent the effective and the initial contact angles, respectively, ϵ_0=8.854x10^{-12} F/m represents the permittivity of free space, ϵ_{d} represents the dielectric constant of the insulator ($\epsilon_{\mathrm{d}} \approx 1$ for water vapor), d represents the thickness of the dielectric ($\approx$ electrode spacing s), σ_{lv} represents the liquid-vapor surface tension (72 mJ/m^2 for water-air), and V represents the applied voltage.

Figure A1 shows θ' for a range of voltages (300 – 1200 V) and spacings (1 - 100 mm) assuming an initial apparent advancing contact angle of 180°. The effective contact angle after the application of voltage was not lower than 170° for $s > 1$ cm. Hence, the effect of the change of surface tension (and subsequently of initial velocity of droplets) was deemed negligible and not considered in my EFE model. However, these effects need to be considered for cases having very small spacings (< 1mm) and high voltages (> 1000V).

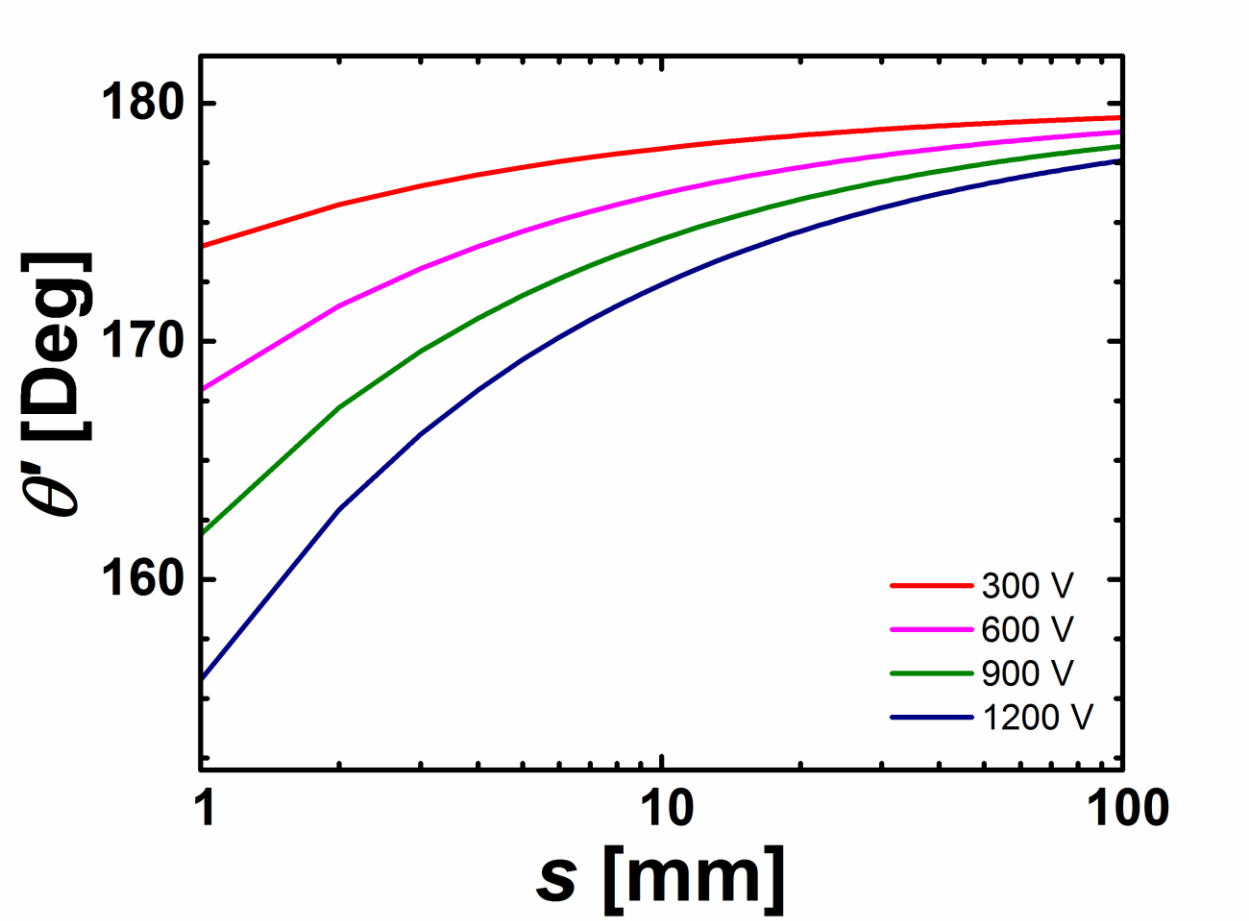

Figure A1. Effective contact angle (θ') due to applied voltage between the superhydrophobic condensing surface and an external electrode. The initial contact angle is assumed to be 180°. The effect of electrode spacing (s = 1-100 mm) and applied voltage (V = 300-1200 V) are calculated using Eq. (A1). For s > 1 cm no relevant change in contact angle is predicted (θ' > 170°).

A.2. Droplet Acceleration Analysis

In this section I propose a complementary explanation (other than the scaling analysis provided in the manuscript) for the behavior observed in Fig. 4a of the manuscript. The analysis is based on the variation of the acceleration, which is a droplet size-independent indicator of motion.

Dividing Eq. (7) of the manuscript by $(4/3)\pi {R_\mathrm{d}}^3 \rho_\mathrm{w}$, we obtain:

$$a_{\mathrm{d,y}} = k{R_\mathrm{d}}^{-1} - g + \frac{q_\mathrm{d} E_\mathrm{y}}{m}, \tag{A2}$$

where k is a factor combining all radius independent properties ($k = -3\rho_\mathrm{v} C_\mathrm{D} sgn(u_{\mathrm{d,x}} + u_{\mathrm{v,x}})(u_{\mathrm{d,y}} + u_{\mathrm{v,y}})^2/8\rho_\mathrm{w}$). From Eq. (S2) we can see that in the high radius limit (R_d > 7 μm, $q_\mathrm{d} \sim {R_\mathrm{d}}^2$), both the electrostatic term and the drag force term decay which leaves only the gravitational term to overcome, hence V_crit increases. In this limit, in order to keep the same acceleration as we increase the droplet size, the electric field should increase linearly with R_d so that the rightmost term in Eq. (S2) becomes independent of R_d. This implies that the critical voltage should increase linearly since it is the only external control variable. However, in the low radius limit, where $q_\mathrm{d} \sim$ constant, the electrostatic term dominates (${R_\mathrm{d}}^3$ dependence in the denominator) hence a large voltage in not needed to attract the droplet to the outer electrode. To better understand the region bridging the two limits, I plotted the acceleration in terms of the droplet radius (Eq. (S2)) for the parallel plate case using the numerical parameters of the initial problem (Fig. A2). Figure S2 exhibits a behavior opposite to the one observed in Fig. 4a, which is logical

since lower acceleration implies higher voltage needed to remove it. Figure A2 shows that the acceleration has a locally minimum at $R_d \approx 8$ μm, due to the complex balance of non-linear forces acting on the droplet in the electric field. A local minimum in acceleration with a negative phase indicates that the droplets are being rapidly decelerated on their trajectory to the outer electrode, meaning that a large electric filed or applied voltage must be used to fully remove them. This is in agreement with my results of Fig. 4a.

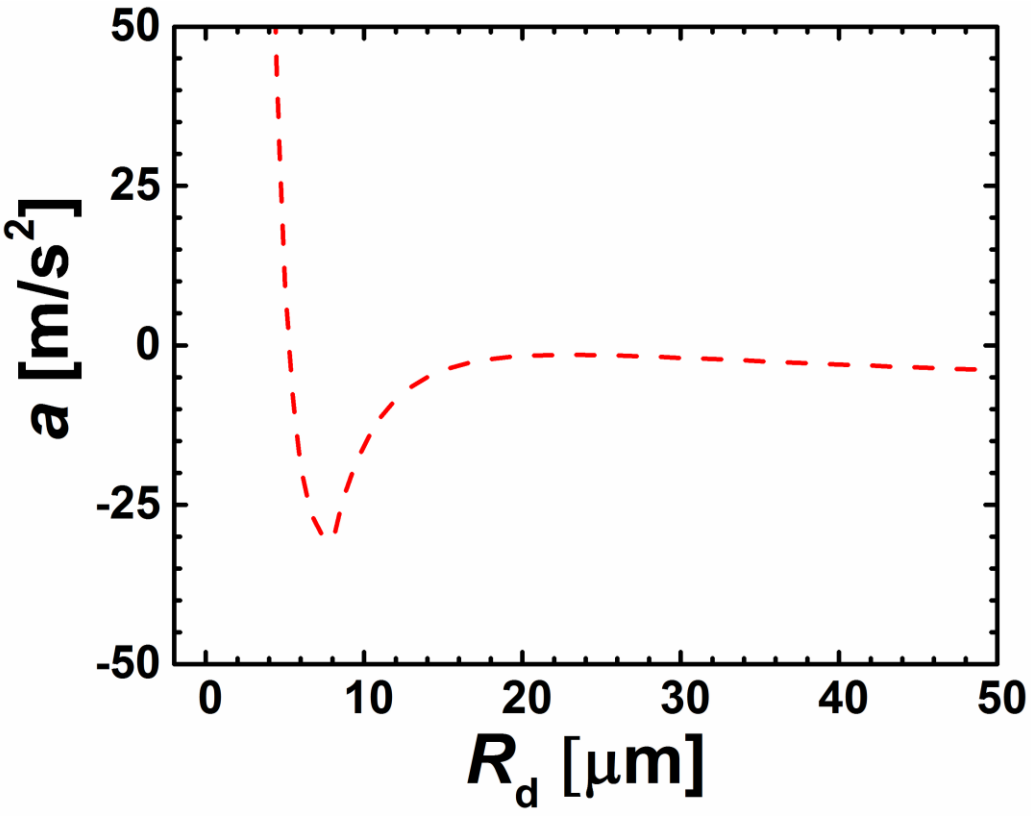

Figure A2. Upward acceleration (a) of a droplet of radius R_d jumping from a superhydrophobic SPF coated flat plate and subjected to an uniform external electric field E = 75 V/cm. The acceleration is found from Newton's second law applied on the droplet experiencing upward electrostatic force and downward drag and gravitational forces. The heat flux and relative vapor flow velocity are considered constant at 0.9 W/cm^2 and 0.2

m/s, respectively. The choice of velocity was aimed to represent the droplet at an intermediate position (0.2 m/s < 0.6 m/s which is the initial relative velocity). The curve gives an explanation for the parallel case behavior observed in Fig. 5a, which can be generalized to both the cylindrical and spherical cases.

A.3. Large Radius Limit of Inner Condensing Electrode

In this section, I validate the consistency of the dependency of the electric field magnitude on the geometry of the electrodes by showing that for a large inner radius of the electrode, all geometries (parallel, cylindrical and spherical) reduce to the parallel plate case (Fig. A3).

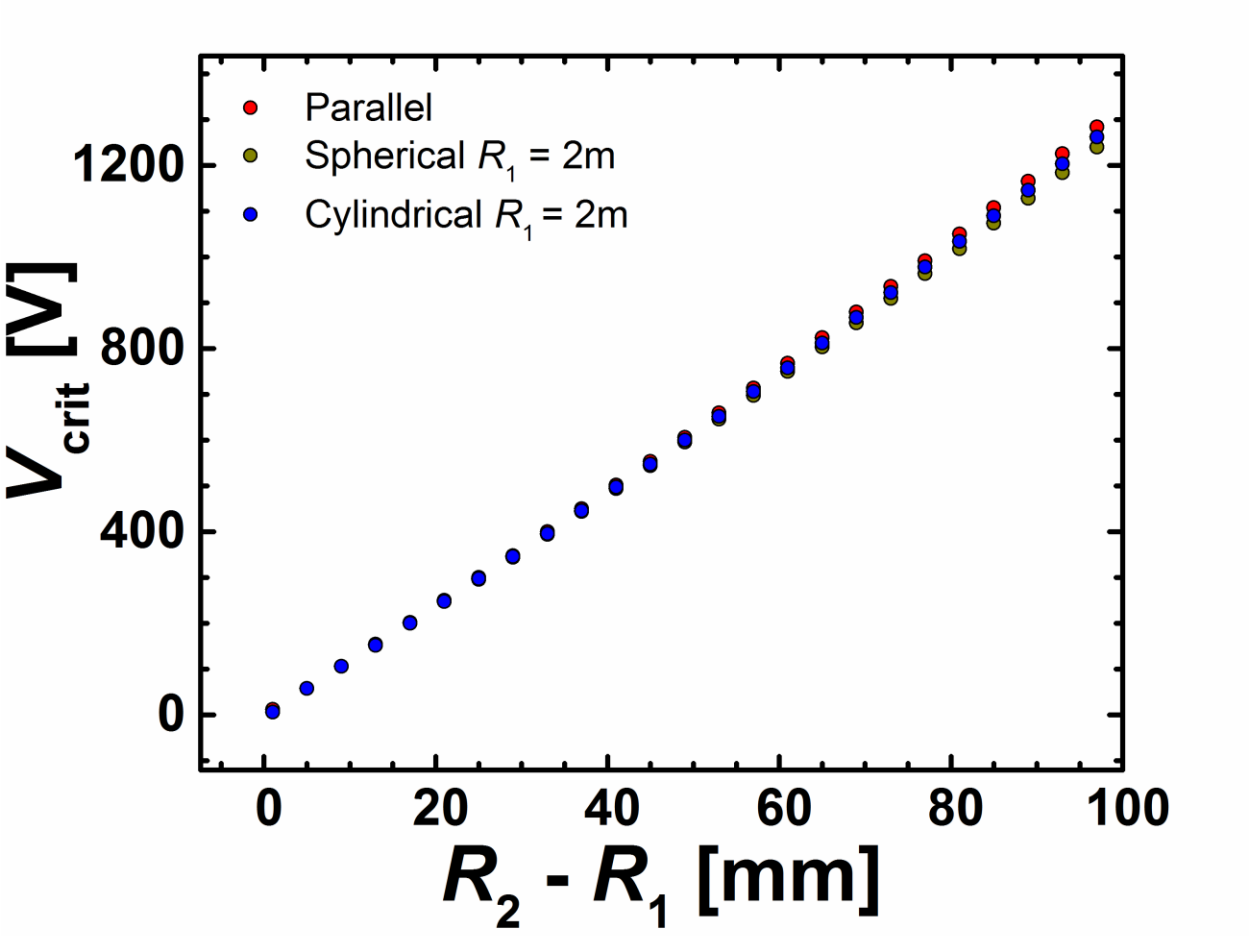

Figure A3. Convergence of the spherical and cylindrical geometries to the parallel plate in the large inner radius (R_1) limit. The critical voltage for droplet removal (V_{crit}) is shown for the three cases in terms of the spacing between the inner and outer electrode (radius R_2). The droplet considered has a 10 μm radius and the heat flux used in the simulation is 0.5 W/cm^2.